AD-A144 150 A STUDY OF THE INTERACTION OF MILLIMETER WAVE FIELDS 1/ 8
WITH BIOLOGICAL SYSTEMS(U) HUGHES AIRCRAFT CO LONG
BEACH CA SUPPORT SYSTEMS A LAWRENCE ET AL. JUL 84
UNCLASSIFIED N00014-83-C-0010 F/G 6/18 NL

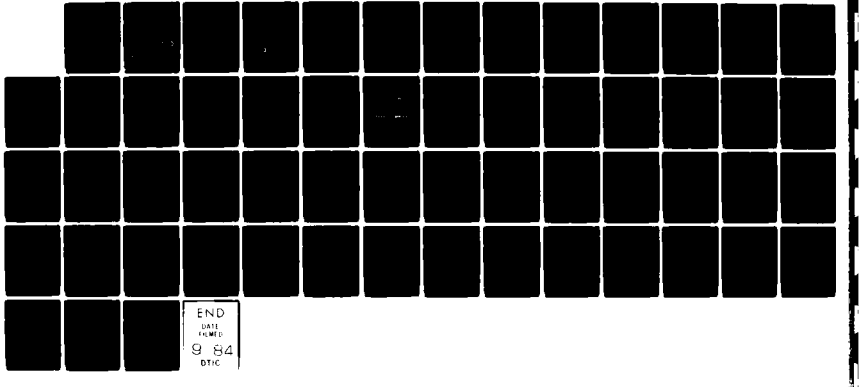

END
DATE FILMED
9 84
DTIC

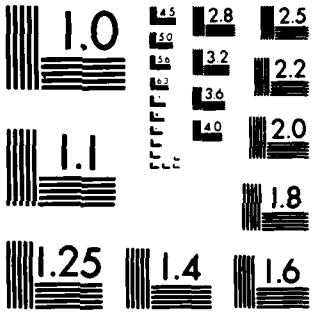

MICROCOPY RESOLUTION TEST CHART
NATIONAL BUREAU OF STANDARDS-1963-A

(213) 513-3000

HUGHES

HUGHES AIRCRAFT COMPANY
SUPPORT SYSTEMS
P.O. BOX 9399
LONG BEACH, CA 90810-0399

12

FINAL REPORT

ONR CONTRACT #N00014-83-C-0010

A STUDY OF THE INTERACTION OF MILLIMETER WAVE FIELDS WITH BIOLOGICAL SYSTEMS

July 1984

Albert Lawrence[a]

Brian Pierce[b]

James McDaniel[b]

David Chang[b]

a) Hughes Aircraft Co.
6155 El Camino Real
Carlsbad, CA 92008

b) Hughes Aircraft Co.
P.O. Box 9399
Long Beach, CA 90810

TABLE OF CONTENTS

ABSTRACT

Our study of the interaction of millimeter wave fields with biological systems has concentrated on Davydov's model of soliton formation in alpha-helices. A qualitative understanding has been obtained for the oscillatory modes of proteins in the millimeter and submillimeter regions of the electromagnetic spectrum. Specifically:

- Four separate groups of frequencies are found to exist in short alpha-helices, ranging from 200 gigahertz to 6 terahertz.
- In long alpha-helices, soliton trapping is predicted for multiquanta excitation at zero temperature, while the existence of solitons at room temperature is called into question.
- A molecular orbital calculation of the exciton-phonon coupling constant in the formamide dimer suggests that the value of this critical constant still needs to be determined.

The results point up the need for further molecular orbital calculations and experimental verification in order to understand the interaction of millimeter waves with biological systems.

FINAL REPORT

A STUDY OF THE INTERACTION OF MILLIMETER WAVE FIELDS WITH BIOLOGICAL SYSTEMS

I. INTRODUCTION

Recent experimental and theoretical work indicates that some biological systems exhibit sensitivities to electromagnetic radiation in the millimeter and submillimeter wavelengths. These fields, even at very low intensities, have been reported to produce profound and marked alterations in a variety of organisms. Specific changes include enhancement and suppression of growth rates in Saccaromyces cerevisiae (1,2), modification of genetic materials in Drosophila, (3), and retardation of free radical reaction rates in Rhodopseudomonas Sphaeroides (4).

In industrial or military environments a significant number of personnel are exposed to electromagnetic fields comprised of two or more frequencies. The need to account for the effects of compound fields places a special burden on biological theory. Research with simple sinusoidal fields indicates that the mechanisms are nonlinear, that both amplitude and frequency are significant in accounting for biological effects. Granting that both amplitude and frequency windows are present for simple sinusoidal fields, the possibilities for compound windows in superpositions of two or more sinusoidal fields increases the number of possible interactions beyond what is reasonable for case-by-case testing. Responses to the extremely low frequency (ELF) range (0.1 to 20000 Hz) and the microwave to submillimeter range (300 MHz to 100 GHz) have particular interest because of the challenge to current theories of interactions between electromagnetic radiation and living tissue.

It is necessary to address the issues from the perspective of the physical sciences in order to establish which biological processes are relevant to the EMF sensitivities of living systems. Adey (5) has recently proposed that the cell membrane is the most likely site of interaction for the electromagnetic field. Adey's model of transmembrane coupling between extracellular fields and intracellular responses leaves unspecified several requirements for an amplifying mechanism between initial cell surface events and resulting enzymatic responses. The first requirement is for an amplification of the weak extracellular electromagnetic fields sufficiently to perturb binding events at the cell surface. The second is for a means to pass a signal through the barrier presented by the cell membrane. The third is for a source of energy to make up the difference between molecular binding energies available at the cell surface and energies released by subsequent intracellular events.

During the past year we have investigated theoretical mechanisms for energy transfer between ambient fields and ions or molecules at the cell surface to proteins in the interior of the cell. Although current research is proceeding toward an unambiguous identification of cell membrane systems involved in the transduction of weak electrical fields (see Adey, (6)) data on the specific proteins involved is presently unavailable. Knowledge of protein structure is essential to a study of protein dynamics; in most cases the analytical work has not yet provided sequences of amino acid residues and is far from yielding the detailed picture of protein structure necessary for a treatment of the molecular dynamics. For this reason we have focussed our research on a structural feature common to all

folded or helical proteins, the amide-I hydrogen bond (-C=O·· H-N-C=). The dynamics of this system are complex, due to electron delocalization on the -C-N-C=O portion of the protein backbone and the nonlinear effective potential at the proton. Both phonon spectra and lines in the amide sequence of acetanilide exhibit a complex pattern of spectral shifts at low temperatures (Johnston, (7)). The pattern of these shifts indicates the presence of coupling between proton vibrations, acoustic phonons and excitations of the C=O and C-N bonds. At the same time the evidence indicates that the effective potential energy of the proton is a double well. The classical or semiclassical dynamics of such nonlinear systems are known to be very sensitive to driving fields at particular frequencies. Because hydrogen bonding in crystalline acetanilide is a good qualitative model for hydrogen bonding in proteins, we should expect to see spectral features in substances composed of alpha-helices similar to those found in acetanilide crystals. This observation would have definite implications for the dynamics of protein molecules. In particular, many of the normal modes of a protein molecule are determined by parameters arising from the hydrogen bonding. If the (-C=O·· H-N-C=) system shows high sensitivity to driving electromagnetic fields in the millimeter wave range, this should be reflected in the dynamics of the whole molecule. As an initial step, we have chosen to investigate a simplified model proposed by Davydov (8) of interactions between amide-I excitations and acoustic phonons in the protein alpha-helix.

A major thesis investigated is that the principal response of biological macromolecules to millimeter wave radiation involves the excitation of acoustic phonons or low frequency vibrations with characteristic frequencies less than 6000 GHz (200 cm-1.) The biological importance of defining the properties of these modes and their interaction with electromagnetic radiation is stressed by indications of their role in the activity of enzymatic proteins (Peticolas, (9), Northrup, et al , (10)) and in directing the paths of hydrogen exchange in proteins (Sheridan, et al (11)). As a result, the understanding of the low frequency dynamics of proteins and polypeptides is the subject of much current experimental (Peticolas, (9)) and theoretical research (Northrup, et al, (10) Sheridan, et al, (11), McCammon and Karplus, (12) Pain, (13), Go, et al, (14), Brooks and Karplus, (15), Davydov, (16,a,b), Hyman, et al, (17), Scott, (18), Lomdahl, (19)). The majority of the theoretical investigations have concentrated on analyzing the low frequency dynamics in terms of such weak interactions as hydrogen bonding, torsional twisting, and van der Waal's forces. Only a few of these studies included a nonlinear coupling between the low energy acoustic phonons and the amide-I vibrational excitons.

Part II of this report covers our investigation of the dynamics of the Davydov model in both short and long chain alpha helices while Part III summarizes results of molecular orbital calculations of the exciton-phonon coupling in the formamide dimer. Our investigation of these two aspects of the Davydov model has provided a qualitative understanding of oscillatory modes of proteins which correspond to the millimeter and submillimeter regions of the electromagnetic spectrum.

II. INVESTIGATION OF THE DYNAMICS OF THE DAVYDOV MODEL

A. BACKGROUND

One of the central issues of bioenergetics is how energy arising from chemical transformations is transferred within enzymes and other protein molecules (Green, (20,21)). The amide-I vibration (C=O stretch) has been proposed as a possible vehicle for energy propagation in biological systems (Green, (21)). A linearized model of amide-I excitation predicts decay to thermal vibrations within a few

picoseconds. This lifetime seems to eliminate propagation of amide-I excitation as an intermediate step in energy transfer. Most chemical processes in enzyme systems involve conformational changes which proceed on relatively leisurely timescales-microseconds or longer.

Davydov (8) has proposed a potential resolution of this disparity. He suggests that the nonlinear character of the interatomic forces can stabilize the amide-I excitations. According to this model, propagation of an amide-I excitation is analogous to an exciton in a one dimensional solid. Excitons are coupled to longitudinal sound waves in this system. This coupling of phonon and exciton fields produces a dynamically stable excitation which propagates as a solitary wave. In essence, the phonons provide a potential well that prevents exciton dispersion. This balance between dispersion and wave steepening is familiar to students of solitonic phenomena. In the continuum approximation, the dynamics of the solitary wave are described by the nonlinear Schroedinger equation, which has solitonic solutions. Davydov's analysis, based on the continuum approximation, demonstrates that this mechanism could stabilize molecular excitons over periods of milliseconds or longer (Davydov, 16a).

Davydov, Eremko and Sergienko (22) derived a phonon-exciton model which more accurately represents the three dimensional arrangement of hydrogen-bonded chains along the protein. Extensive numerical calculations based on this model confirm that Davydov's continuum approximation is qualitatively correct for alpha helical chains containing several hundred peptide residues. All models exhibit solitary waves, which form at some threshold value for the coupling between excitons and phonons. Further, the solitary waves are very stable and closely resemble solitons.

There are several issues which need to be resolved before Davydov's model can be rigorously applied to proteins in a living cell. These issues fall into four categories. The first issue is the range of chemical or dynamical phenomena to which the Davydov model can be applied legitimately. The second issue is whether a model related to the Davydov model may be useful for structurally complex proteins. The third issue is the relevance of the parameters used in previous modeling efforts. The strength of the exciton-phonon coupling is particularly significant. The fourth issue is the behavior of the model at temperatures commonly found in living organisms.

Davydov originally proposed his model to account for muscle contraction (Davydov, (8)). Because muscle contraction is thought to involve a conformational change in a long-chain protein, we must determine whether the Davydov model allows for a substantial portion of the excitonic energy to be transferred to phonons or large-scale nuclear motions. Unfortunately, numerical calculations show that only a small portion of the total energy resides in the phonons associated with the solitary wave (Scott, (18)). Even though the Davydov model closes the gap in timescales between dispersion of amide-I excitation and conformational changes in proteins, the gap in energy remains quite wide. Because energy transfer from an exciton mode to a highly excited phonon mode involves many quanta, the probability of energy transfer from an exciton mode to a highly excited phonon mode remains quite small (Ovchinnikov and Erikhman, (23)). Nevertheless, the Davydov model remains a reasonable candidate for the transfer of bond energy.

The necessity of application of the Davydov model to a wide range of protein structures arises because only a small fraction of the proteins in living systems exist as long alpha-helical chains. More general models of excitonic propagation

are necessary for the highly folded forms which are found in enzymes, microfilaments, and chemical receptors. Lomdahl (19) has proposed one such model. This model reduces to the Davydov model for short alpha helical segments.

The dynamics of the Davydov model are very sensitive to the effective force represented by the phonon-exciton coupling. Previous numerical studies have taken the value for the formamide dimer calculated by Kuprievich and Kudritskaya (24) as representative. This value was obtained from an ab-initio self-consistent field computation. The authors did not report on the details, which is unfortunate because such calculations are quite sensitive to choice of the equilibrium geometry, basis sets, or configuration interaction level. Our calculations indicate the value reported by Kuprievich and Kudritskaya may underestimate the true value by as much as a factor of two. We conclude that an accurate assignment of the coupling constant remains to be established (See part III, below).

Another related problem arises in the extrapolation of experimental results obtained with hydrogen-bonded molecular crystals, such as acetanilide (Careri, et al , 25)) to support the Davydov model for proteins. The Davydov model includes only exciton-phonon coupling terms which are linear in the phonons. Many of the models of propagation of excitons in molecular crystals include coupling terms which are quadratic. These terms are necessary to account for phonon frequency changes which may be present in addition to changes in the equilibrium positions of the molecules (Munn and Silbey, (26)). Spectrographic results obtained at cryogenic temperatures (Johnston, (7,a,b)), indicate that the phonon frequency in acetanilide is shifted by a change in the position of the proton in the hydrogen bonds of crystalline acetanilide.

The thermalization problem has been addressed by Davydov (Davydov, (27)). By using a density matrix approach, he has been able to show that the effective phonon-exciton coupling constant is decreased by the presence of thermal phonons (Davydov, 27, 28). The magnitude of this effect remains to be computed. In fact, there is no conclusive evidence, either theoretical or experimental, which would indicate whether Davydov solitons exist at physiological temperatures. Our results indicate that thermal effects may prevent the formation of Davydov solitons in vivo .

B. THEORETICAL DERIVATION OF THE MODEL

Davydov's original model (Davydov, (8)) is a chain of N molecules along the z-axis. The equilibrium positions are given by:

$$z_o = nR_o + u_n \tag{1}$$

where R_o is the equilibrium distance between molecules and u_n is the displacement of the nth molecule from equilibrium. The Hamiltonian operator for excitons (amide-I bond excitations in the alpha helix) may be written:

$$H_{ex} = \Delta \Sigma_n P_n^+ P_n - J \Sigma_n (P_{n+1}^+ P_n + P_n^+ P_{n+1}) \tag{2}$$

In this formula Δ is the molecular excitation energy and J is the energy of resonant interaction of neighboring molecules. These quantities may be described in terms of a two-level model of the amide-I bond. (Fedyanin and Yakushevich, (29,a,b)). In this representation the states of the bond are denoted 0 and f. The excitation energy of an isolated molecule is written as ϵ .

Then:

$$\mathcal{L} = \Delta\varepsilon + 2D;\quad D = \langle f0|V_{n,n+1}|f0\rangle - \langle 00|V_{n,n+1}|00\rangle$$
$$J = \langle 0f|V_{n,n+1}|f0\rangle \tag{3}$$

We may also write:

$$J = \left(\frac{1}{4\pi\varepsilon_c}\right)\left(\frac{d^2}{R^3}\right) \tag{5}$$

where d is the dipole moment of the molecules. The operators P_n and P_n^+ are the annhilation and creation operators satisfying the Pauli commutation relations:

$$[P_n, P_m^+] = \delta_{nm}(1-2P_n^+P_n)$$
$$[P_n, P_m] = 0 \tag{5}$$
$$P_n^2 = 0.$$

The phonon Hamiltonian has the form

$$H_{ph} = \frac{1}{2M}\sum_n p_n^2 + \frac{w}{2}\sum_n (u_n - u_{n-1})^2 \tag{6}$$

where p_n is the momentum conjugate to the displacement u_n:

$$[u_n, p_m] = i\hbar\delta_{nm}. \tag{7}$$

If the mass of the molecule is M then

$$w = Mv_\alpha^2 = (Mv_\alpha^2)/(R_0^2 \tag{8}$$

where w is the elastic coupling constant of the chain and v_α is the sound velocity. The dispersion relation for phonons is given by

$$\Omega_q = 2v_\alpha|\sin(qR_0/2)| \tag{9}$$

where q is the wave vector and Ω_q is the phonon frequency. The interaction of excitons with phonons is given by

$$H_{int} = \chi\sum_n P_n^+P_n(u_{n+1} - u_{n-1}) \tag{10}$$

where χ is the exciton-phonon coupling parameter. The total Hamiltonian for the model is

$$H_{sol} = H_{ex} + H_{ph} + H_{int}\quad . \tag{11}$$

A particular solution for the time-dependent Schroedinger equation associated with H_{sol} is given by the following wave function:

$$|\Psi_s(t)\rangle = \sum_n [C_n(t)\exp\{\sigma(t)\}P_n^+|0\rangle\quad . \tag{12}$$

In this expression $C_n(t)$ is the probability amplitude of an exciton occupying site n at time t. Conservation of energy implies the normalization condition

$$\sum_n |C_n(t)|^2 = 1 . \tag{13}$$

The operator

$$\sigma(t) = i/\hbar \sum_n [\xi_n(t)p_n - \pi_n(t)u_n] \tag{14}$$

is derived from a coherent state representation for the phonons. This follows from the relations:

$$\begin{aligned} u_n &= \sum_q (\hbar/2MN\Omega_q)^{1/2} (b_q + b_{-q}^+) \exp(inq) \\ p_n &= -i\sum_q (\hbar\Omega_q M/2N)^{1/2} (b_q - b_{-q}^+) \exp(inq) . \end{aligned} \tag{15}$$

Substitution of these identities into the expression for $\sigma(t)$ gives an expression of the form

$$\exp\{i/\hbar(\Omega_q z_q(t) b_q + z_q^*(t) b_q^+)\} \tag{16}$$

where

$$\begin{aligned} z_q = (\hbar/2MN\Omega_q)^{1/2} \sum_n \pi_n \exp(inq) + \\ i(\hbar\Omega_q M/2N)^{1/2} \sum_n \xi_n \exp(inq) . \end{aligned} \tag{17}$$

The properties of the coherent state representation imply that the functions $\pi_n(t)$ and $\beta_n(t)$ represent the average momentum and displacement respectively of the nth molecule.

Explicit expressions for the functions $\beta_n(t)$, $\pi_n(t)$ and $C_n(t)$ can be derived via Hamilton's canonical equations applied to the energy functional. The energy functional is defined as follows:

$$F = \langle H_{sol} \rangle = \langle \Psi_s(t) | H | \Psi_s(t) \rangle . \tag{18}$$

We may calculate F from the definitions:

$$\begin{aligned} F = {} & \Delta \sum_n |C_n(t)|^2 - J \sum_n [C_{n+1}^*(t) C_n(t) + C_{n+1}(t) C_n^*(t)] \\ & + (1/2M) \sum_n \pi_n^2(t) + \frac{w}{2n} \sum [\beta_n(t) - \beta_{n-1}(t)]^2 \\ & + \chi \sum_n |C_n(t)|^2 [\beta_{n+1}(t) - \beta_{n-1}(t)] . \end{aligned} \tag{19}$$

The canonical Hamilton's equations

$$\dot{\pi}_n(t) = \frac{\partial F}{\partial \beta_n} \qquad \dot{\beta}_n(t) = \pi_n(t)/M \tag{20}$$

yield the identify

$$\frac{\partial^2 \beta_n(t)}{\partial t^2} = (1/M)\ \frac{\partial \pi_n(t)}{\partial t} = \tag{21}$$

$$\frac{W}{M}[\beta_{n+1}(t) + \beta_{n-1}(t) - 2\beta_n(t)] +$$

$$(\frac{\lambda}{M})[|C_{n+1}(t)|^2 - |C_{n-1}(t)|^2]$$

If we write the phonon energy

$$W = \frac{1}{2M}\sum_n \pi_n^2(t) + \frac{W}{2}\sum_n [\beta_n(t) - \beta_{n-1}(t)]^2 , \tag{22}$$

then Schroedinger's equation implies

$$i\hbar \frac{\partial C_n(t)}{\partial t} = \frac{\partial F}{\partial C_n^*(t)} =$$

$$\{\lambda + W\lambda[\beta_{n+1}(t) - \beta_{n-1}(t)]\}\ C_n(t) -$$

$$J[C_{n-1}(t) + C_{n+1}(t)] \tag{23}$$

Equations (21) and (23) describe the dynamics of a single chain.

The equations for a single chain may be generalized to the case of three interacting chains as in a protein alpha helix. In this model, resonance interactions may occur along the protein helix. Adding these interactions to the model yields a system of coupled equations in which the dynamic variables are indexed by spine number as well as position along each hydrogen-bonded spine.

Our calculations are based on a coupled system of ordinary differential equations, obtained as outlined in the previous section. Except for choice of boundary conditions, our procedures are formally equivalent to those of Hyman, McLaughlin and Scott (17). The ends of the helix are not mechanically constrained. The complete model is given by the following system of equations

$$\frac{idC_{n,i}}{dt'} = (1.41)\ C_{n,i}[(d\beta_{n,i}/dt')^2 + (\beta_{n+1,i} - \beta_{n,i})^2]$$

$$- 0.058\ (C_{n-1,i} + C_{n+1,i}) + 0.092(C_{n,i+1} + C_{n,i-1})$$

$$+ 0.372\ (10^{10}\chi)[(1-\delta_N^n)\ (\beta_{n+1,i} - \beta_{n,i})C_{n,i}$$

$$+ (1 - \varepsilon_o^n)\ (\beta_{n,i} - \beta_{n-1,i})C_{n,i} + (1-\delta_N^n)C_{n+1,i}\ x$$

$$(\beta_{n+1,i} - \beta_{n,i}) + (1 - \varepsilon_o^n)C_{n-1,i}(\beta_{n,i} - \beta_{n-1,i})]$$

$$\frac{d^2\beta_{n,i}}{dt'^2} = (1-\varepsilon_N^n)(-\varepsilon_{n+1,i} + \varepsilon_{n,i}) \tag{24}$$

$$+ (1-\varepsilon_o^n)(\varepsilon_{n,i} - \varepsilon_{n-1,i}) + 0.132(10^{10}) \times$$

$$\{(1-\varepsilon_N^n)(1-\varepsilon_o^n)[|C_{n+1,i}|^2 - |C_{n-1,i}|^2]$$

$$+\varepsilon_o^n[|C_{1,i}|^2 + |C_{o,i}|^2] - \varepsilon_N^n[|C_{n-1,i}|^2 + |C_{n,i}|^2$$

$$+ C^*_{n+1,i}(C_{n+1,i} - C_{n-1,i}) + (C^*_{n+1,i} - C^*_{n-1,i})C_{n,i}\}$$

We have normalized the time variable in these equations by setting $t' = (w/M)^{1/2} t$. The quantities δ_o^n, δ_N^n account for the boundary conditions at the n = 0 and n = N ends of the helix respectively.

For the computations on short alpha helices, one quantum of amide-I excitation energy was assumed to be located at the (0,1) position at the initiation of the simulation. No provision was made for random motions due to thermal disorder during the course of the computations. As in the work of Scott (18), the only free parameters of the model are the number of peptide residues in the alpha helix and the nonlinear coupling coefficient between excitons and phonons. During the course of the computations, we used values of 0.2×10^{-10}, 0.4×10^{-10}, and 0.6×10^{-10} Newtons for chain lengths of 18, 24, 27, 30, and 60 peptide residues.

For the calculations on the long alpha helices one, two and three quanta initializations for the exciton energy were employed. Chain length was 200 residues, coupling constant ranged from 0.5×10^{-10} Newtons to 3.0×10^{-10} Newtons. Calculations were carried out for the chain initially at rest and for phonon motion simulating a temperature of 300° Kelvin.

The resulting systems of differential equations were solved on a VAX 11/780 using double precision arithmetic. All integrations were performed using a third-order Adams-Bashford-Moulton predictor-corrector method (Shampine and Gordon, (30)). The code was set to maintain a relative error of 0.000001 at each time step during the computation. Computation of the total probability of bond occupancy

$$P = \sum_{n,1} |A_{n,1}|^2$$

served as an independent check of accuracy. In every computation P - 1 was maintained at a value less than 0.00001.

C. RESULTS

1. SHORT ALPHA HELICES

The total phonon energy was plotted as a function of time in order to examine the energy exchange between excitons and phonons. Examination of the plots for the fifteen combinations of chain length and coupling constants described above shows that several time scales are present:

a) Short period oscillations (about 3-6 terahertz). These may be seen as transient bursts which recur at periodic intervals.

b) The time interval between the appearance of the bursts is roughly proportional to the chain length. The duration for each burst appears to be independent of chain length. Figures 1-3 show plots of total phonon energy for chain lengths of 18, 27 and 36 residues. The high frequency oscillations recur at 3×10^{-12} seconds for chain length 18, 4.5×10^{-12} seconds for chain length 27 and 6×10^{-12} seconds for chain length 36.

c) Intermediate period fluctuations (500 gigahertz to 1 terahertz). The time period for these fluctuations is proportional to chain length. Intermediate period fluctuations are marked in Figures 2 and 3.

d) Long period fluctuations (100 gigahertz). Long period fluctuations are seen for chain lengths of 27 and 36 residues. The clearest example may be seen in Figure 2 for a chain length of 27 residues, with coupling coefficient 0.4×10^{-10} Newtons. This oscillation persists for many cycles in the original record from which the figure is extracted.

Reordered according to frequency, the four separate timescales observed are:

a) Fast oscillations, 3 to 6 terahertz, occuring in bursts.

b) Intermediate fluctuations, 500 to 1000 gigahertz.

c) Recurrence of bursts, 200 to 500 gigahertz.

d) Long period fluctuations below 200 gigahertz.

Examination of the modules of the Fourier transform of the total phonon energy confirms these observations. As the chain length is increased, the short period oscillations become less significant and the long period oscillations more significant. This trend is shown in Figures 4 and 5. The division between the timescales is seen most clearly for a chain length of 27 residues.

Phonon Spectra

Because phonon energy in an actual protein alpha helix is not easily subject to direct experimental observation, we also computed the $\pi(t)$ momentum expectation function for selected residues along the chain. The modulus of the Fourier transform of $\pi(t)$ gives the phonon spectrum, as may be seen from equation (15) and the relation $\pi_n(t) = \langle \psi_s(t) | p_n | \psi_s(t) \rangle$ (See Haaken, 31). In order to analyze the collective modes, we evaluated the sum of momenta for residues 1, 2 and 3 and the sum of momenta for residues [n/2], [n/2] - 1 and [n/2] - 1 and [n/2] - 2.

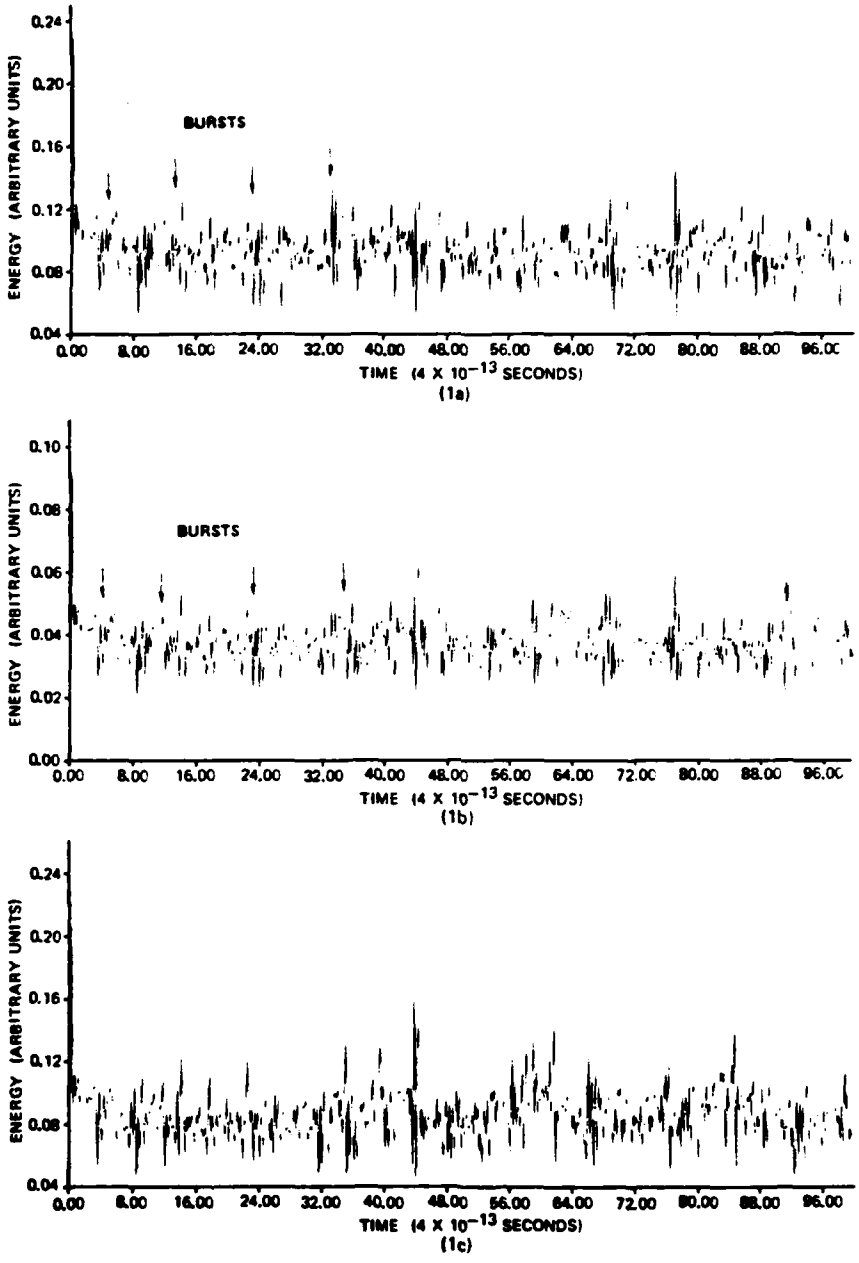

Figure 1. Phonon energy for an 18 residue chain. Coupling coefficients: a) 0.2×10^{-10}, b) 0.4×10^{-10}, c) 0.6×10^{-10} Newtons. Bursts of 6 Thz oscillations may be seen at time intervals of approximately 3.2×10^{-12} seconds. Bursts are indicated by arrows.

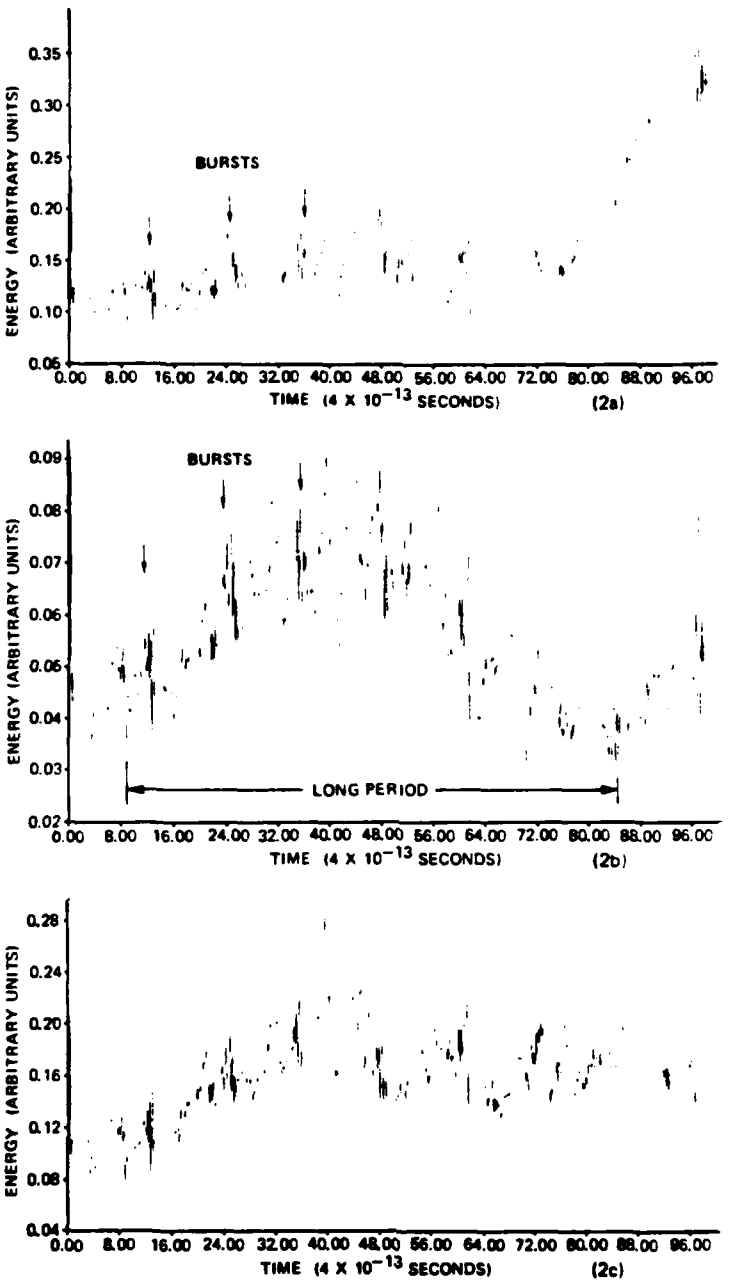

Figure 2. Phonon energy for a 27 residue chain. Exciton-phonon coupling coefficients are as in Figure 1). Bursts of 6 Thz oscillations may be seen at time intervals of approximately 4.8 X 10^{-12} seconds. Location of bursts indicated by arrows above traces. Periodicity of intermediate-time scale fluctuations is indicated by arrows below the traces. A long-period fluctuation is indicated on b).

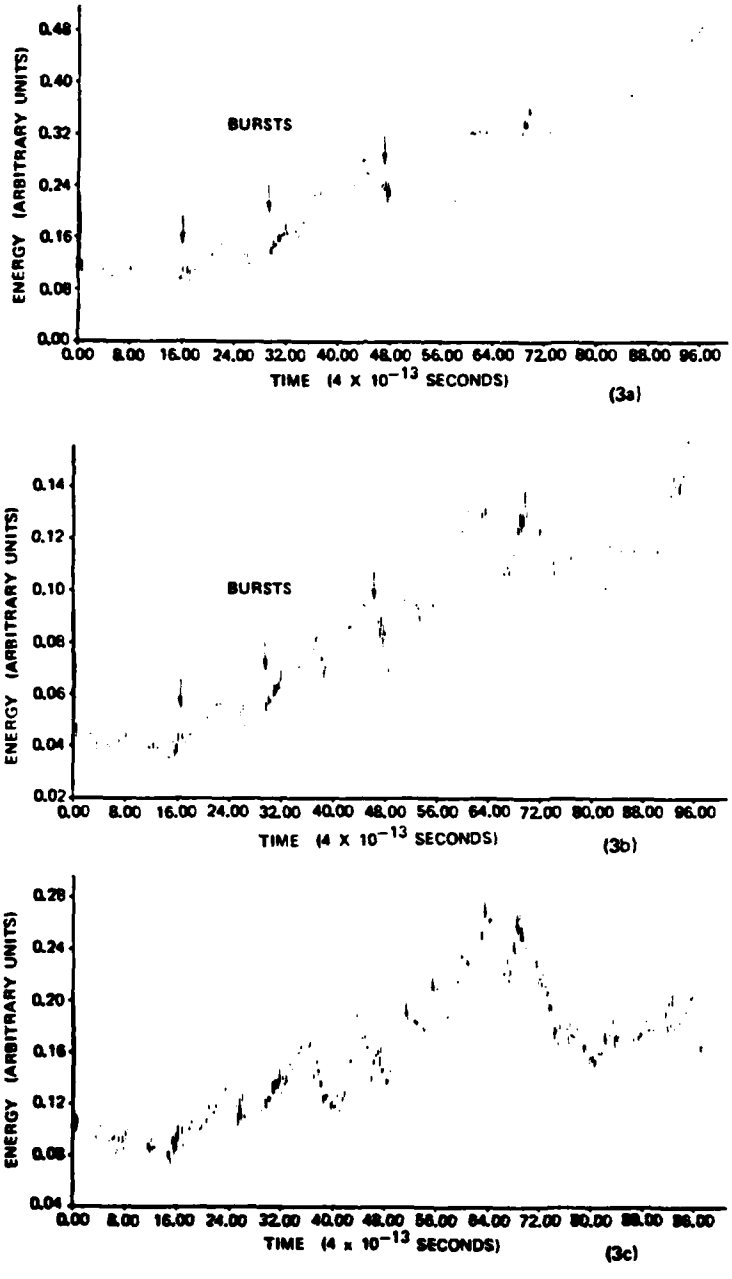

Figure 3. Phonon energy for a 36 residue chain. Coupling coefficients as in Figure 1). Bursts of 6 Thz oscillations may be seen at time intervals of approximately 6.4 X 10^{-12} seconds. Periodicity of bursts indicated by arrows above traces.

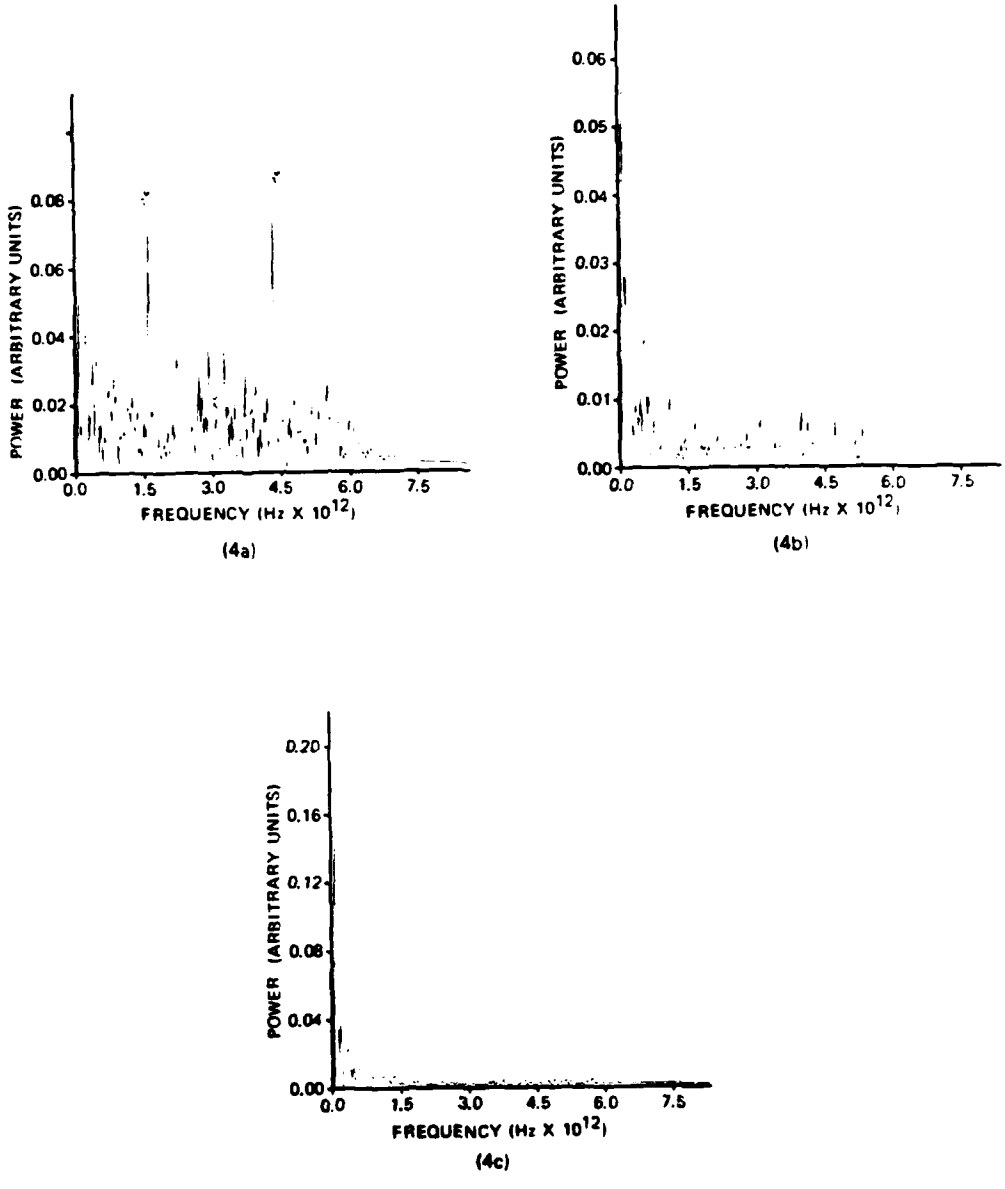

Figure 4. Fourier transforms of total phonon energy. Phonon energy for chains of a) 18 residues, b) 27 residues, and c) 36 residues. Nonlinear coupling coefficient is 0.2×10^{-10} Newtons. Note the trend toward lower frequencies for longer chains.

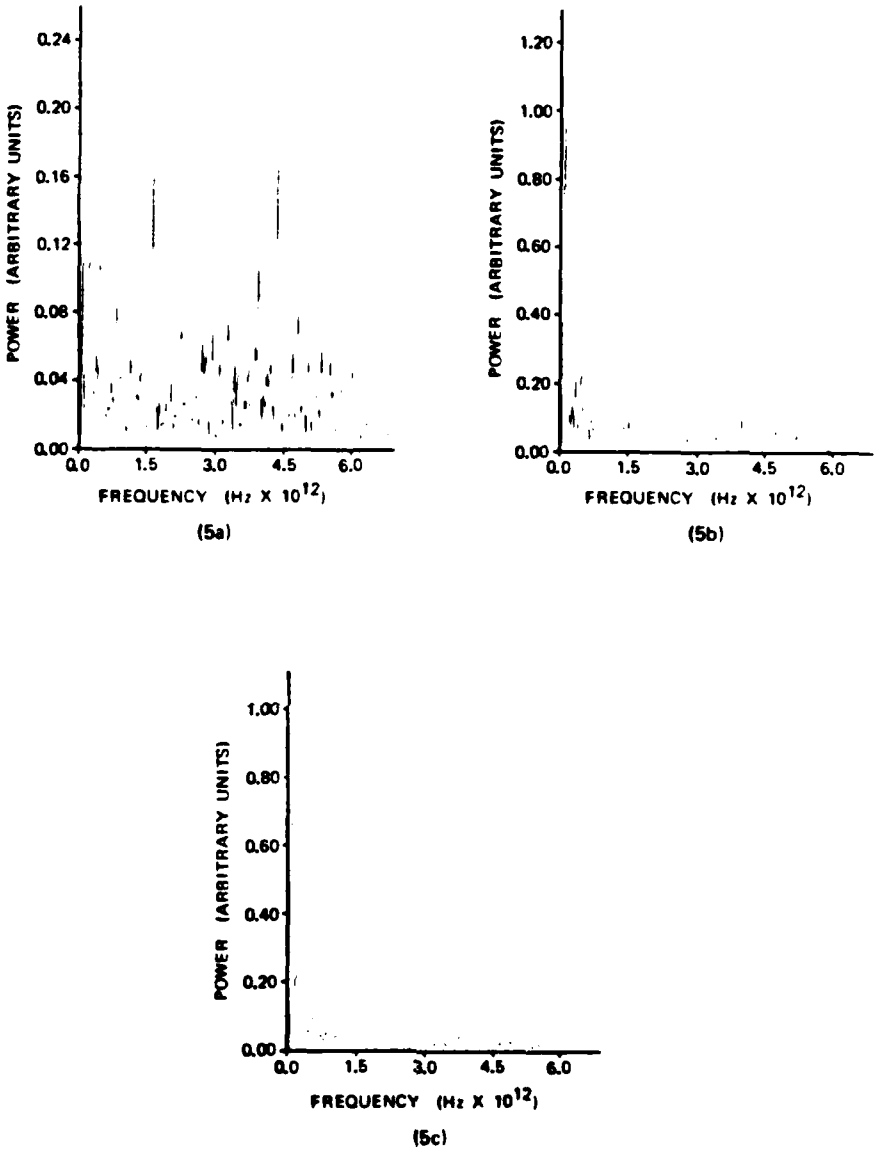

Figure 5. Fourier transforms of total phonon energy data. Phonon energy for chains of a) 18, b) 27 and c) 36 residues. Nonlinear coupling coefficient is 0.6×10^{-10} Newtons. Frequency scale is as in Figure 4.

Samples of the momenta plots are shown in Figure 6. We also computed the modulus of the Fourier transform of each momentum plot. Plots of amplitude versus frequency are shown in Figures 7, 8 and 9. Each of the plots consists of a series of well-defined peaks. These peaks correspond to the normal modes of the corresponding linear chains, and follow the same dispersion relation as given in equation (9).

2. LONG ALPHA HELICES

Our finding on long alpha helices are summarized in Figures 10-17. (Each of these plots required more than 10 hours of CPU time to produce.) As may be seen from Figures 10, 11 and 12, representing evolution of probability of exciton occupation subsequent to initial excitations of one, two and three quanta of amide-I excitation energy placed in the end peptide groups of chains at 0^{o}Kelvin, soliton formation is a function of excitation level. Even in the case of two or three quanta, there is a significant probability that a fast-moving dispersive wave will form. This may be seen by the sharply-defined ripples which form upon reflection of the wave from the end of the chain. Another branch of the dispersion of excitations, which is indicated by waves similar to but moving more slowly than the main solitary wave. Note that the coupling constant in this case is 0.5×10^{-10} Newtons, a value which is reported by Scott (18) to be in the middle of the range of coupling constants at which solitary waves form.

The second series of Figures, 13, 14 and 15, illustrate the effects of high coupling constants. Figure 13, which represents evolution of exciton probability in a chain at 0 degrees Kelvin with a coupling coefficient of 1.5×10^{-10}Nt, shows that a slowly-moving solitary wave may form at a lower excitation level in the case of stronger coupling. Figure 14, also representing exciton evolution at 0 degrees Kelvin but at a coupling constant of 3.0×10^{-10}Nt, shows that at very high levels of excitation, a randomly-moving exciton forms. This is familiar to solid-state physicists, in that phonons scattering from the exciton push it from site to site. Figure 15, representing evolution subsequent to a two quanta excitation, shows eventual trapping of the exciton at the end of the chain. A similar phenomenon has been reported by Scott (18), with the major difference that the exciton did not initially leave the end of the chain.

Figures 16 and 17 illustrate the effects of thermalization. Figure 16, shows the evolution subsequent to a two quanta excitation in a chain with thermal phonon motion representing a temperature of 238^{o} Kelvin. The excitons disperse rapidly, within 20 picoseconds. Figure 17 shows exciton evolution subsequent to three quanta excitation in a chain with a phonon temperature of 300 degrees. Dispersion is also rapid in this case.

D. DISCUSSION

1. SHORT ALPHA HELICES

We believe that the full range of phenomena observed during the course of our modeling studies requires a more detailed analysis than the passage to the continuum limit which is common to the literature on the Davydov model (Davydov, 8, 16, 27, 28, Scott, 18). A more accurate treatment should follow the spirit of Toda's analysis of nonlinear lattices. (Toda, 32).

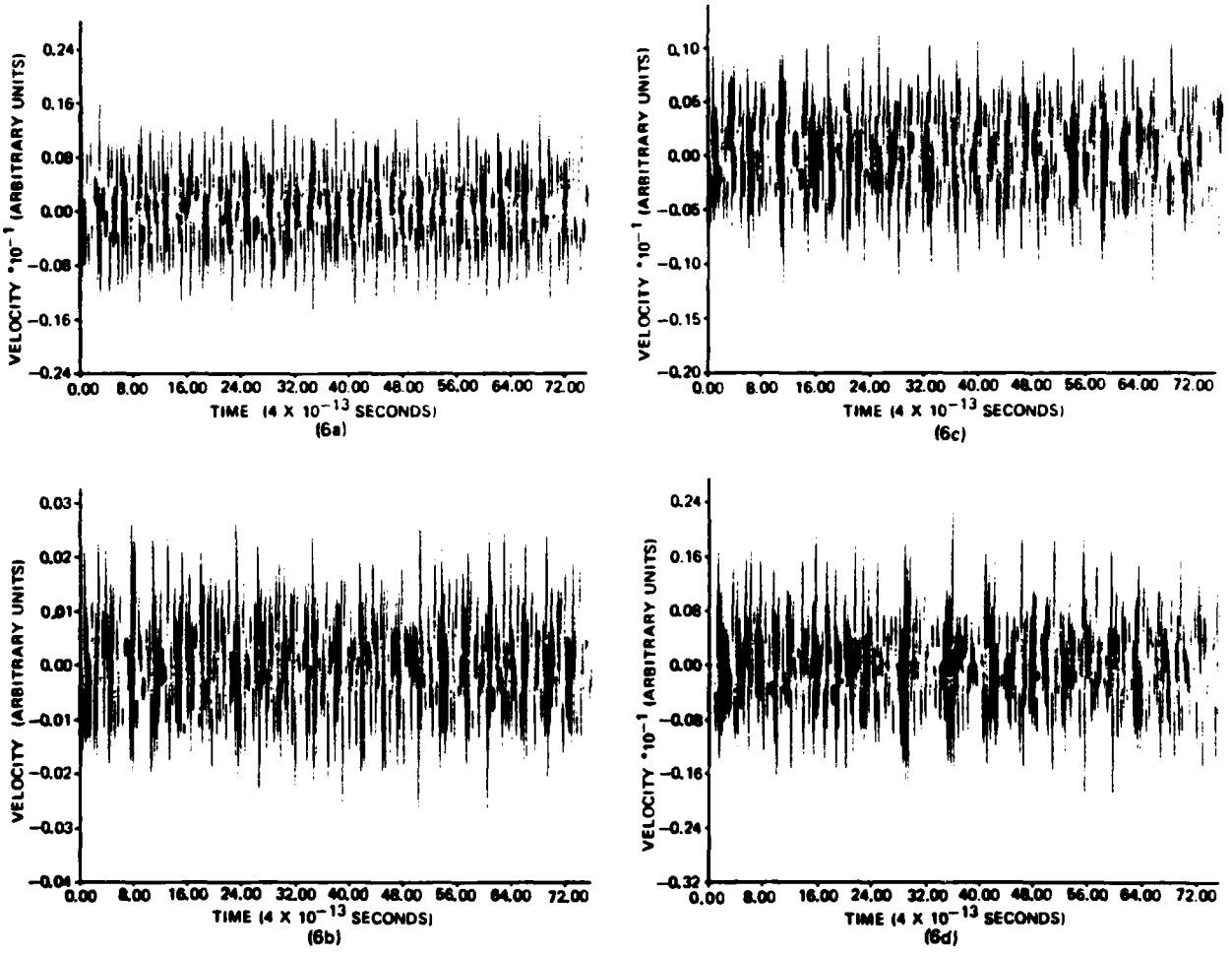

Figure 6. Velocity of displacement for groups at mid-section of alpha helices of a) 18, b) 30, c) 36 and d) 60 residues. Nonlinear coupling coefficient is 0.2×10^{-10} Newtons.

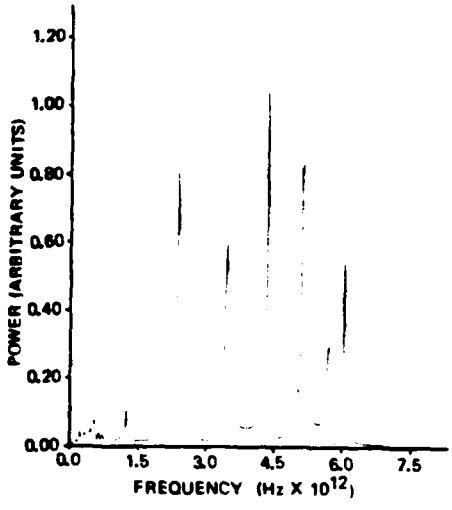

(7a)

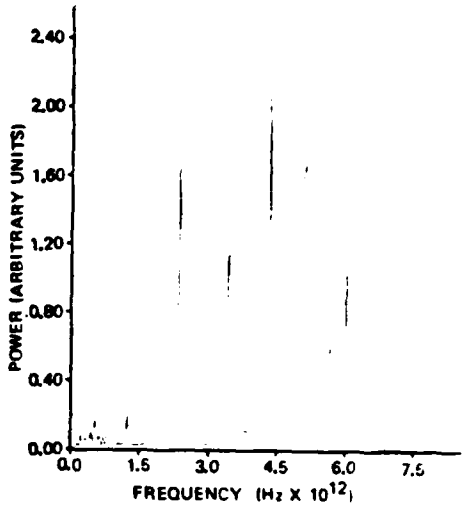

(7b)

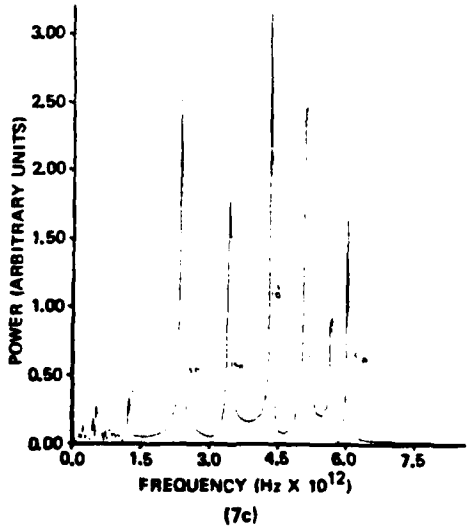

(7c)

Figure 7. Phonon spectra. Chain length, 24 residues. Site is midchain. Nonlinear coupling coefficients are a) 0.2, b) 0.4, c) 0.6 $X10^{-10}$ Newtons. Note that relative amplitudes and positions of peaks remain the same. Horizontal scale in terahertz. Vertical scale is arbitrary.

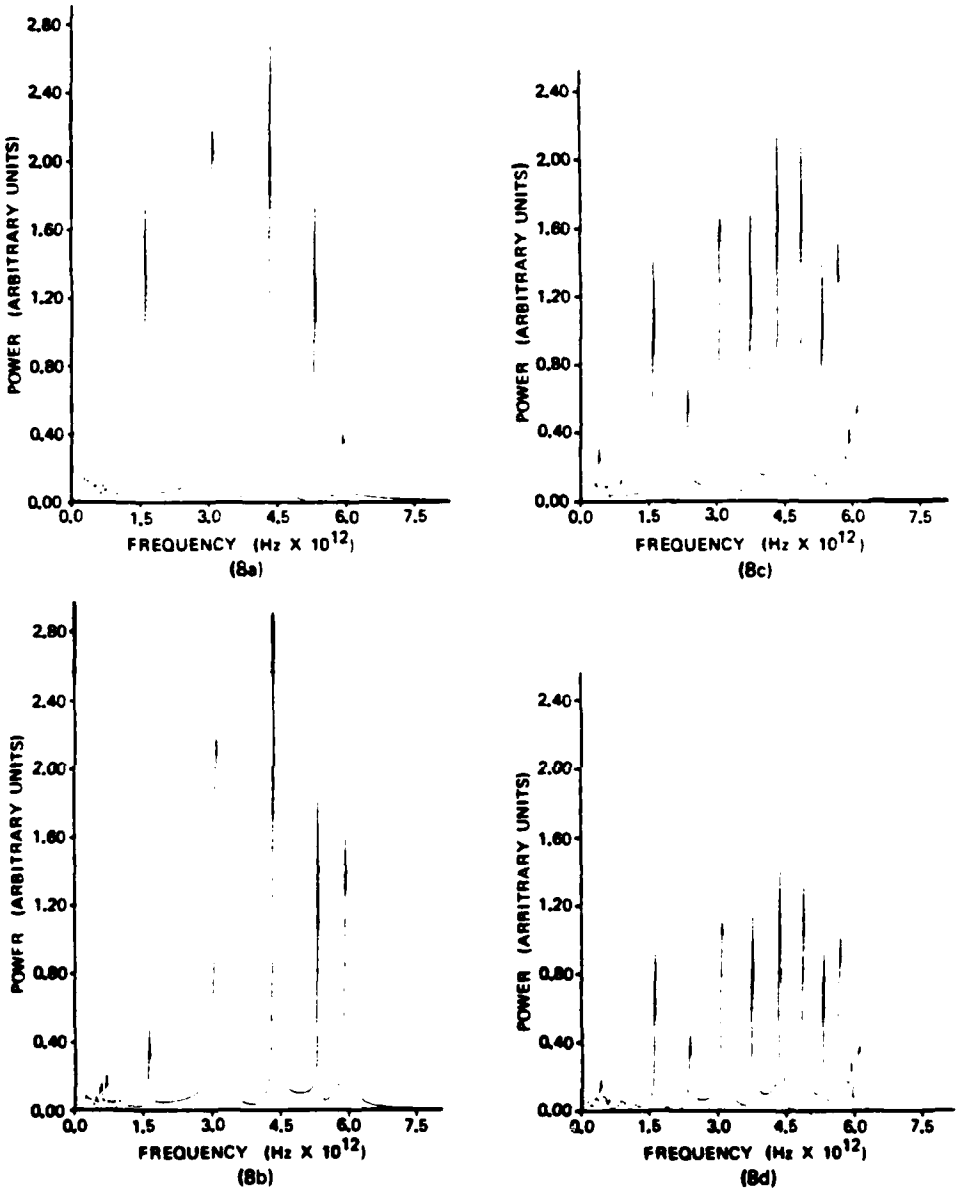

Figure 8. Phonon spectra. Same scales as in Figure 7). Chain lengths and sites are a) 18 residues, end, b) 18 residues, middle, c) 36, middle, d) 36, end. Coupling coefficient is 0.4×10^{-10} Nt. Note that peaks are in the correct harmonic relationship.

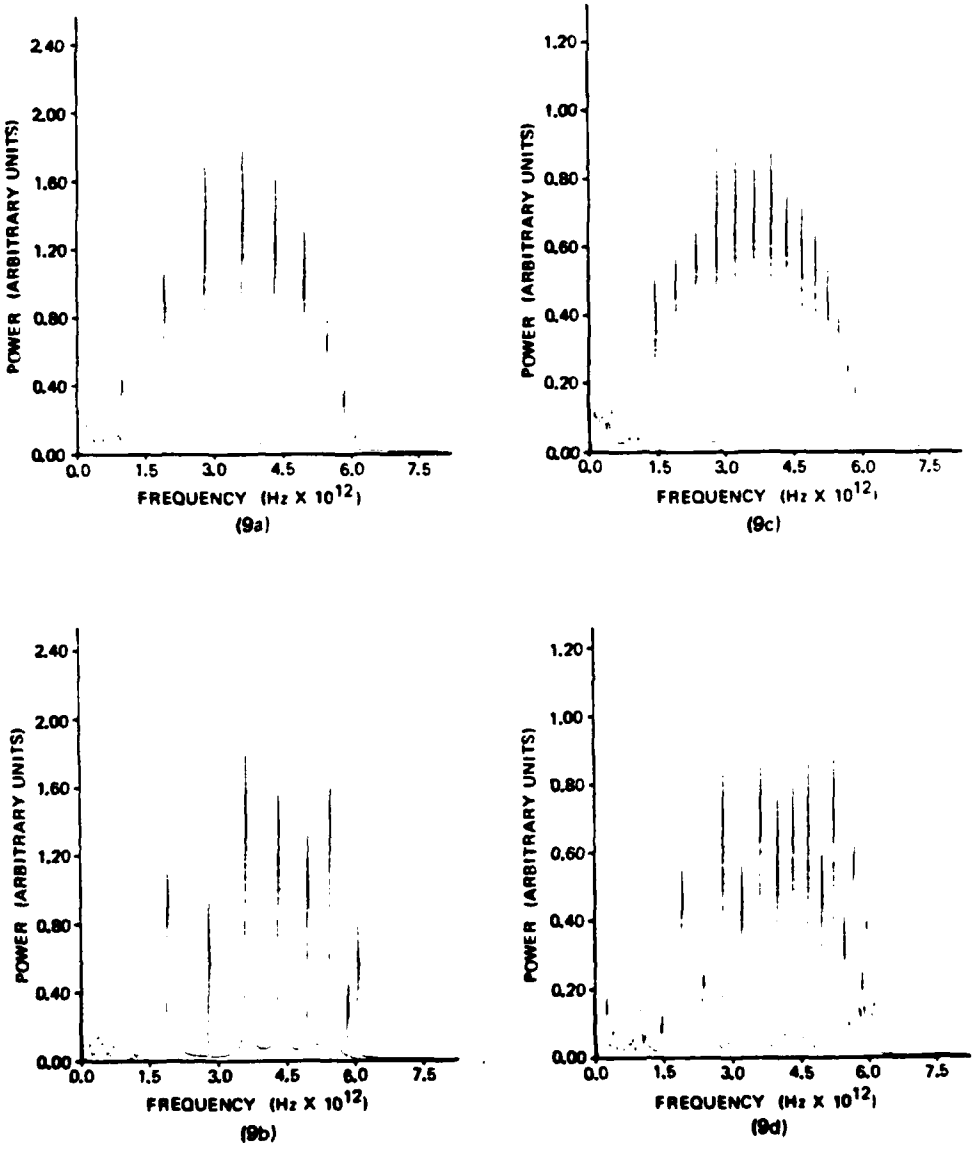

Figure 9. Phonon spectra. Same scales as in Figure 7). Chain lengths and sites are a) 30, end, b) 30, middle, c) 60, end, d) 60, middle. Coupling coefficient is 0.4×10^{-10} Nt.

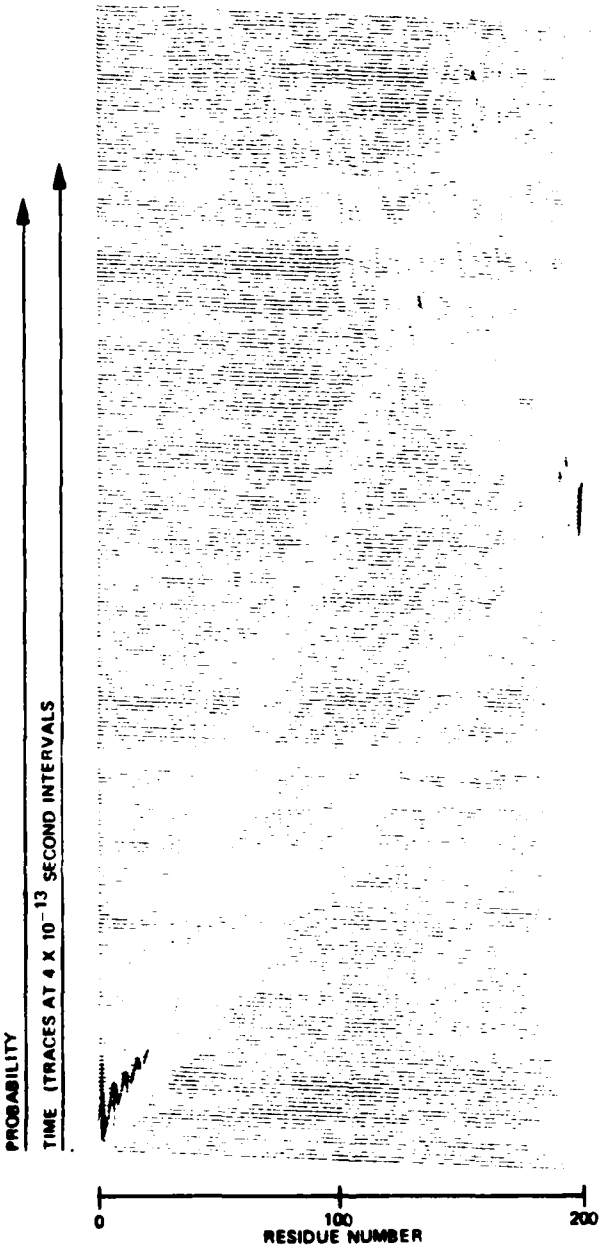

Figure 10. Plot of probability of exciton occupation. Horizontal axis is position along a chain of 200 residues. Each trace represents a time increment of approximately 0.4 picoseconds. Phonon-exciton coupling parameter is 0.5 x 10^{-10} Nt. Note that most of the excitonic energy propagates as a dispersive wave.

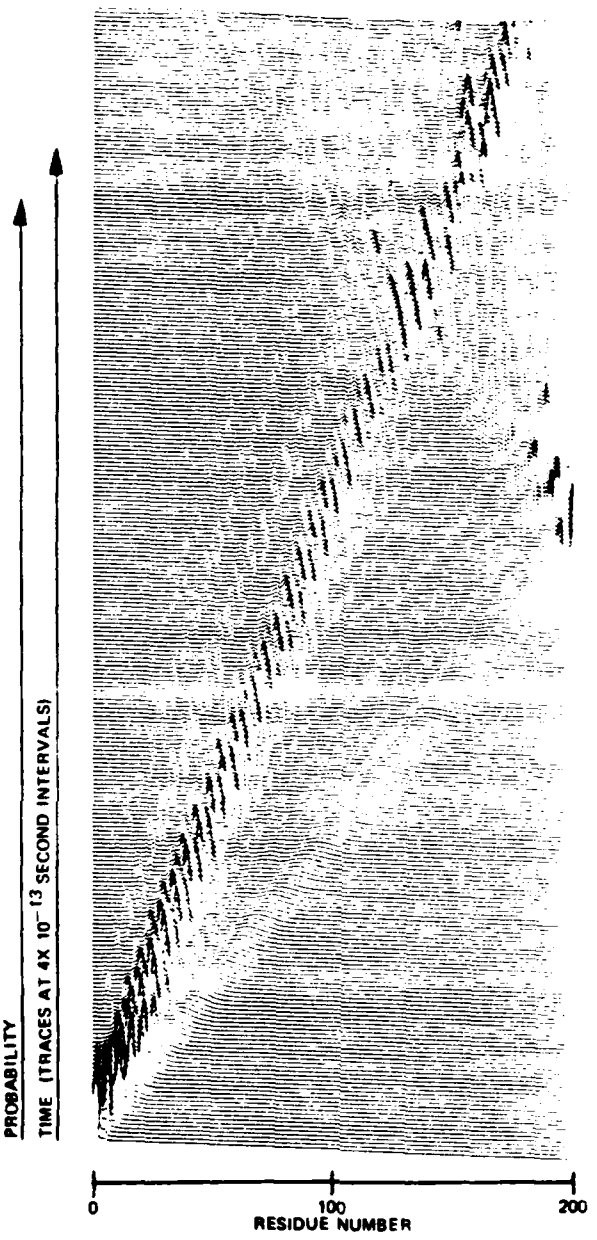

Figure 11. Plot of probability of exciton occupation. Coupling constant of 0.5×10^{-10} Newtons, two quanta initialization. Note the presence of both a solitary wave and a faster-moving dispersive wave.

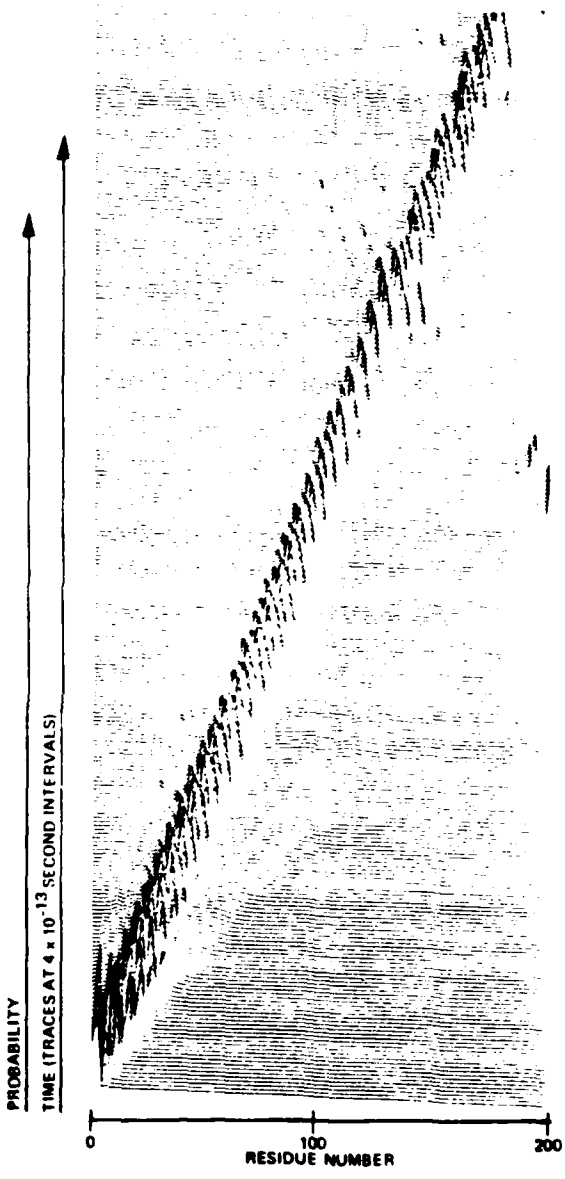

Figure 12. Evolution of exciton occupation probability. Coupling constant of 0.5×10^{-10} Newtons, three quanta initialization.

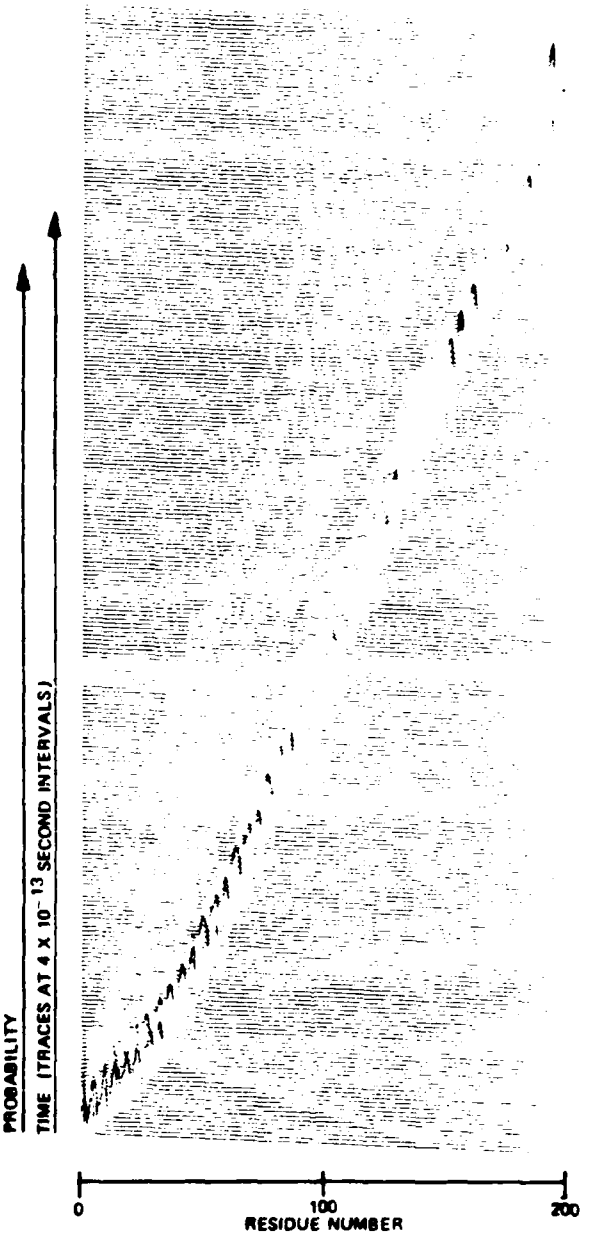

Figure 13. Evolution of exciton occupation probability. Coupling constant of 1.5×10^{-10} Newtons, one quantum initialization.

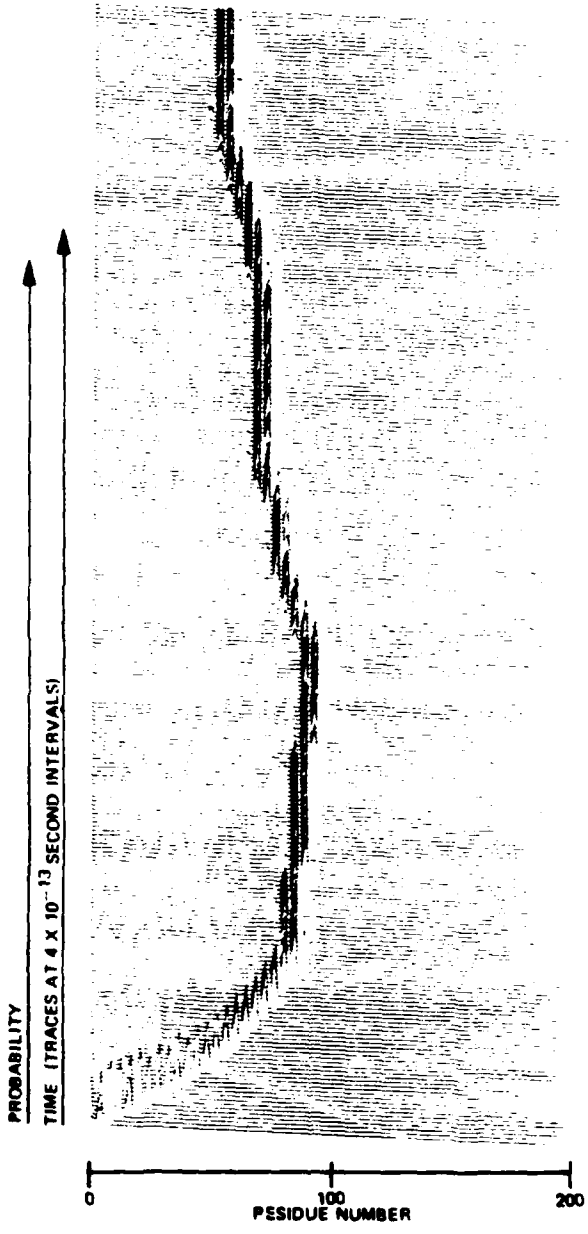

Figure 14. Evolution of exciton occupation probability. Coupling constant of 3.0×10^{-10} Newtons. One quantum initialization. Note that a solitary wave forms in this case.

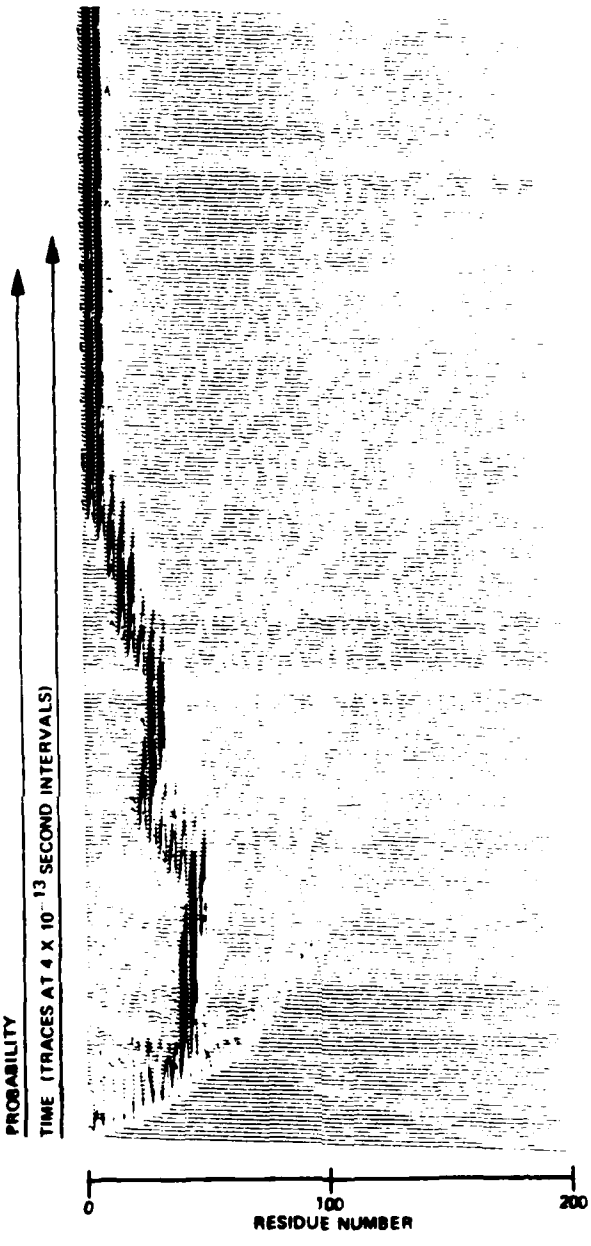

Figure 15. Evolution of exciton occupation probability. Coupling constant of 3.0×10^{-10} Newtons. Two quanta initialization. Note that a self-trapped exciton is attracted to chain boundary.

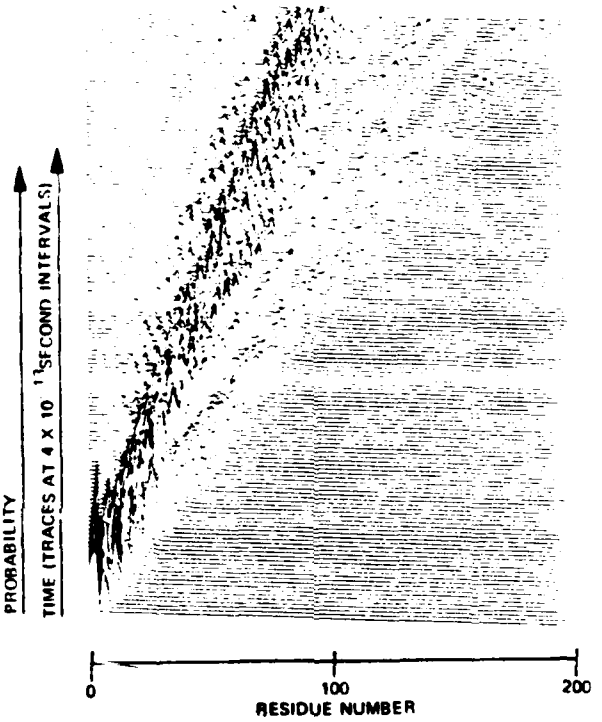

Figure 16. Evolution of exciton occupation probability. Coupling constant of 0.5×10^{-10} Newtons. Three quanta initialization. Phonon temperature of 300^{o} Kelvin. Note rapid dispersion of excitons.

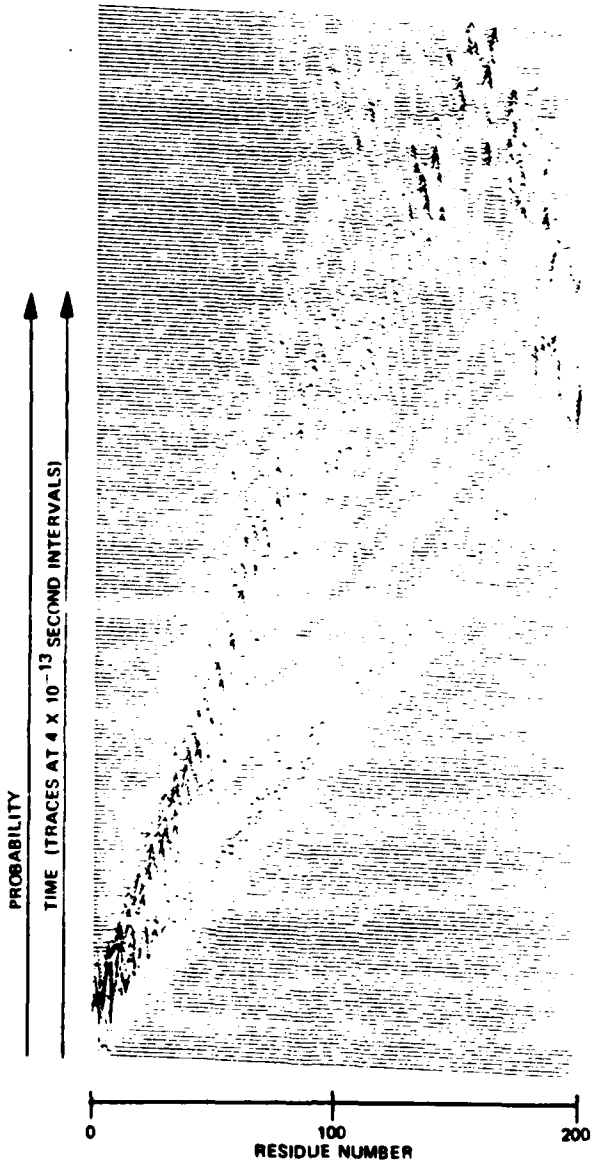

Figure 17. Evolution of exciton occupation probability. Coupling constant of 0.5×10^{-10} Newtons. Two quanta initialization. Phonon temperature of 238° Kelvin. Excitons disperse rapidly.

Equations (24) may be simplified by neglecting coupling terms of small magnitude. In the first equation, this includes the observation that only the hydrogen bond on the C=O side of the peptide unit will influence the amide-I energy:

$$\frac{idC_{r,i}}{dt'} = 0.372(10^{10}\chi)[(\varepsilon_{n+1,i} - \varepsilon_{n,i})C_{n,i} + (\varepsilon_{n,i} - \varepsilon_{n-1,i})C_{n-1,i}$$

$$- 0.058(C_{n+1,i} + C_{n-1,i}) + 0.092(C_{n,i+1} + C_{n,i-1}) \qquad (25)$$

$$\frac{d^2\varepsilon_{n,i}}{dt'^2} = 2\varepsilon_{n,i} - \varepsilon_{n+1,i} - \varepsilon_{n-1,i} + 0.132(10^{10}\chi)[|C_{n+1,i}|^2 + |C_{n-1,i}|^2]$$

For the sake of simplicity, we have not included the end conditions in these equations. These equations, which have several features in common with Flaschka's equations for the Toda lattice (Flaschka, 33), may be treated as matrix equations. To begin the analysis, note that to the first order the equations for the excitons and phonons are uncoupled. The equations for the excitons may be written as a system of linear autonomous equations:

$$i/dA/dt' = KA, \qquad (26)$$

with solution $A = \exp(iK)A_0$.

The phonon displacement is given in turn by an approximate equation:

$$id^2\mathcal{B}/dt'^2 = K\mathcal{B} + F, \qquad (27)$$

where $\mathcal{B}_{n,i}$ is given by $iB_{n,i} + B_{ni}$) and F is the nonlinear term given by the excitons. The solution of (27) is given by the formula

$$\mathcal{B}(t) = \int_0^t \exp[-iK(t-\mathcal{T})]F(\mathcal{T})d\mathcal{T}. \qquad (28)$$

This scheme may be continued self-consistently to improve the estimate of the evolution of the exciton probability amplitude, given by equation (27), but equation (28) accounts for the major features we have noted in the results section. For example, the average lifetime of an exciton at a site of the chain is about 1.6 picoseconds. An exciton moving along the chain will excite 1.6 phonons most strongly when it is near one of the ends of the chain. This is the origin of bursts in the phonon mode at about 6 THz. Other fluctuations are due to resonances between phonons and the periodicity of the excitons. The long period observed for the chain length of 27 residues is due to transfer between even and odd-numbered spines of the alpha helix.

Because the calculated phonon spectra do not reflect the frequency shifts observed in acetanilide crystals, we suggest that the interaction term of the Hamiltonian should include a quadratic term. Writing

$$H'_{int} = \sum_n P_n^+ P_n (u_{n+1} - u_{n-1}) + G \sum_n P_n^+ P_n (u_{n+1} - u_{n-1})^2 \quad (29)$$

would yield a new expression for the energy functional

$$F' = F + G \sum_n |C_n|^2 [\varepsilon_{n+1}(t) - \varepsilon_{n-1}(t)^2] \quad (30)$$

Equation (23) would be modified by addition of a term

$$\frac{2G}{M} \{ |C_{n+1}|^2 [\varepsilon_{n+2}(t) - \varepsilon_n(t)] - |C_{n-1}(t)|^2 [\varepsilon_n - \varepsilon_{n-1}(t)] \} \quad (31)$$

Similar modifications may be made in the three-spine model.

2. LONG ALPHA HELICES

Mathematical analysis of the complicated dispersion observed for a single quantum excitation is not yet complete. The reason for soliton formation in the case of two and three quanta excitation may be seen from the fact that phonon formation goes as the square of the number of excitons and thus the "feed-back" term in the exciton evolution equation (25) increases as the cube of the number of excitons. The qualitative change in exciton dynamics observed when the coupling constant reaches 3.0×10^{-10} Nt is also due to a qualitative change in the "feed-back" term. In this case, the coefficient of the feedback term exceeds unity.

III CALCULATION OF THE EXCITON-PHONON COUPLING CONSTANT

A. BACKGROUND

The calculation of the non-linear coupling between the vibrational excitons localized in amide-I bonds and the phonons in the hydrogen-bonded "spines" of a polypeptide alpha-helix is important to the understanding of the propagation of undispersed amide-I vibrational excitons along these "spines". An undispersed exciton which propagates through an interaction with phonons is also defined as a Davydov soliton. In a numerical analysis of a polypeptide alpha-helix of finite length, Scott showed that a Davydov soliton can be sustained when the exciton-phonon coupling parameter exceeds a minimum magnitude of 0.35×10^{-10} Nt(18). The question of the validity of this threshold is addressed in the calculations described below.

According to Kuprievich and Kudritskaya, the exciton-phonon interaction parameter consists of a resonance component (X_2) and two non-resonance components (X_1^+,X_1^-)(24). The X_2 term can be obtained from the known magnitude of the resonance interaction between the transistion dipoles associated with the amide-I vibration in alpha-helical polypeptides (44). In this manner, Scott derived a value of 10^{-12} Newtons for X_2(18). The non-resonance components are best determined from a theoretical treatment of exciton-phonon coupling at the microscopic level. This treatment involves the use of the quantum mechanical <u>ab initio</u> self-consistent field (SCF) molecular orbital (MO) procedure. The exciton-phonon coupling terms and the application of <u>ab initio</u> SCF MO theory to the calculation of these terms are discussed in greater detail in Section III B. Section III C presents our preliminary calculation of X_1^+ and that of Kuprievich and Kudritskaya (24) for the simplest hydrogen-bonded polypeptide - the formamide dimer. Conclusions are presented in Section III D.

The Hamiltonian for the interaction of vibrational excitons with acoustical phonons in a discrete chain of N molecular units forming a regular one-dimensional lattice was derived by Kuprievich and Kudritskaya (24, 34), in a form differing slightly than that reported by Davydov.

$$H_{int} = \sum_{m=1}^{N} P_m^+ P_m [X_1^+ (u_{m+1} - u_m) + X_1^- (u_m - u_{m-1})] + \sum_{m=2}^{N} (P_m^+ P_{m-1} + P_{m-1}^+ P_m) X_2 (u_m - u_{m-1}) \quad (32)$$

In this expression, P_m^+ and P_m are the creation and annihilation operators of vibrational excitation in the unit m, u_m is the displacement of this unit from its equilibrium position, X_1^+ and X_1^- are the parameters defining the non-resonance interaction of a unit with its neighbors, and X_2 is the parameter defining the resonance interaction for two neighboring units in a chain. Note that the terms in the first sum with X_1^- at m=1 and with X_1^+ at m=N should be omitted, because both terminal molecular units have only one neighbor.

The explicit formulations of X_1^+, X_1^-, and X_2 for a dimeric group consisting of peptide groups m and m+1 are as follows (24, 34):

$$X_1^+ = (\hbar/2w)\,\partial(\partial^2 E_{m,m+1}/\partial Q_m^2)/\partial R_{m,m+1} \quad (33)$$

$$X_1^- = (\hbar/2w)\,\partial(\partial^2 E_{m,m+1}/\partial Q_{m+1}^2)/\partial R_{m,m+1} \quad (34)$$

$$X_2 = (\hbar/2w)\,\partial(\partial^2 E_{m,m+1}/\partial Q_m \partial Q_{m+1})/\partial R_{m,m+1} \quad (35)$$

where w is the intramolecular amide-I vibrational frequency, $R_{m,m+1}$ is the distance or hydrogen-bond length between groups m and m+1 (See Figure 18a), $E_{m,m+1}$ is the interaction energy (or total energy in the Born-Oppenheimer approximation(35)) of groups m and m+1, and Q_i is the normal mode coordinate for the amide-I vibrations in groups i=m and m+1. Since the second derivatives of the total energy of the dimer with respect to its vibrational normal coordinates are proportional to the harmonic force constants for these modes, the coupling parameters in Eqs. (33) - (35) can be viewed as the first derivatives of the harmonic force constants for the amide-I vibrations in the dimer with respect to the intermolecular distance $R_{m,m+1}$. Thus, the acoustical phonons of the alpha-helix which are defined principally by changes in $R_{m,m+1}$ (i.e., changes in the pitch of the alpha-helix (24, 34)) are coupled to the amide-I vibrational excitons.

As stated in the Introduction, a value of 10^{-12} Nt for X_2 can be derived from the known magnitude of the resonance interaction between the amide-I vibrational transition dipoles (18). Kuprievich and Kudritskaya argue that X_1^- is negligible with respect to X_1^+ (24). The principal reason is that the dominant contribution to the amide-I vibrational normal mode in a peptide group is the C=O bond stretching motion (24, 36, 37). As a result, the amide-I vibration of group m will be much more perturbed than that of group m+1 by changes in $R_{m,m+1}$. This observation is clearly seen in Figure 18a. The major objective of our analysis of the exciton-phonon coupling in polypeptides will therefore be the calculation of X_1^+.

B. QUANTUM-MECHANICAL CALCULATION OF THE NON-RESONANCE EXCITON-PHONON INTERACTION PARAMETER X_1.

The calculation of the interaction energy of the two peptide groups ($E_{m,m+1}$) as a function of the intra- and inter-molecular coordinates is fundamental to the determination of X_1^+. In the Born-Oppenheimer or adiabatic approximation (35), the interaction energy is equivalent to the total energy (E) for the system, which is calculable using quantum mechanical ab initio self-consistent field (SCF) molecular orbital (MO) procedures. The details of these procedures and their application to the study of the electronic structure of atoms and molecules are well-covered by Schaefer in his book (38) and the references therein.

The mapping of the E surface for a dipeptide system as a function of its intra- and inter-molecular coordinates is a formidable task. However, as outlined by Kuprievich and Kudritskaya (24), one can obtain a crude estimate of X_1^+ by the following procedure. 1) Investigate the simplest system that contains two peptide groups connected by a hydrogen bond, i.e. the formamide dimer shown in Figure 18b. 2) Determine an equilibrium geometry for the dimer. 3) Approximate the amide-I vibrational normal mode as only a C=O bond stretching motion. As a result, the Q_m in Eq (33) becomes $\delta\sqrt{K/w}$ (24), where δ is the change in C=O bond length away from its equilibrium value (positive/negative δ signifies an expansion/contraction of the

(18a)

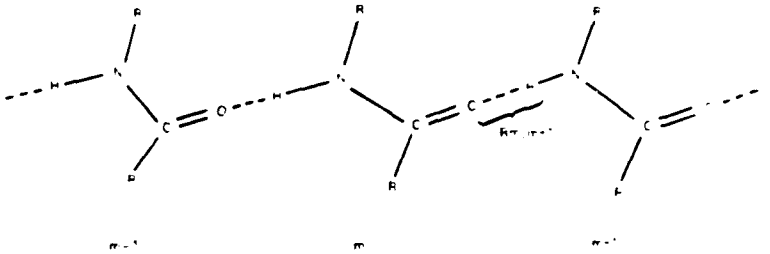

(18b)

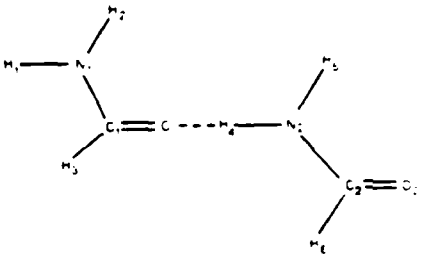

(18c)

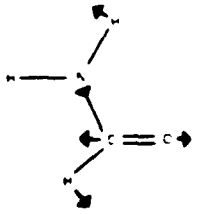

Figure 18 (a). Structure of a chain of hydrogen-bonded peptide groups. Unspecified molecular fragments are designated R in the figure. Note that the integer m represents one peptide group. The hydrogen bond length between groups m and m+1 is indicated by $R_{m,\ m+1}$.

Figure 18 (b). Structure of the formamide dimer and numbering of the atoms used in the calculations.

Figure 18 (c). Description of the vibrational normal mode in the formamide monomer which contains the stretching motion of the C=O bond. This figure is taken from Ref 37, and the direction and length of the arrows represent the activity of the given atoms in the normal mode.

C=O bond), K is the harmonic force constant for the C=O bond stretching motion, and w is the amide-I frequency. Eq. (33) then takes the form

$$X_1^+ = (\hbar w/2K)\, \partial K/\partial R_{m,m+1} \qquad (36)$$

where $K = \partial^2 E/\partial \xi^2$. 4) Calculate E at three different values of ξ and estimate $K = \partial^2 E/\partial \xi^2$ by $\Delta(\Delta E)/(\Delta \xi)^2$. 5) Calculate K at different values of $R_{m,m+1}$ and estimate $\partial K/\partial R_{m,m+1}$ by $\Delta K/\Delta R_{m,m+1}$. In summary, a crude determination of X_1^+ for a polypeptide chain can be made by calculating the total energy of the formamide dimer in different geometries and then taking the appropriate numerical derivatives.

Both Kuprievich and Kudritskaya's (24) and our ab initio SCF MO calculations of the total energy of the formamide dimer were performed with the minimal atomic orbital basis set composed of 36 Slater-type orbitals (STO), each being approximated by 3 Gaussian functions (3G) (39). It is stressed that the STO-3G basis set is good only for qualitative analyses of the geometries of amide compounds (37, 38). For example, an energy-minimized geometry of the formamide monomer calculated using the STO-3G basis set was not in complete agreement with the experimentally determined geometry for the molecule (37). The major differences were that the calculated geometry was slightly non-planar, while the observed one was planar, and that the calculated C-N bond length was 0.1Å longer than the observed one (see Table I and Ref. (37)). Although the STO-3G basis set has its limitations with regard to the accurate study of molecular properties, SCF convergence was achieved for all 6 of geometries of the formamide dimer, and the cost per calculation was about 12 minutes of CPU time on the VAX 11/780. Thus, the STO-3G basis set allows one to make a qualitative estimate of X_1^+ with the least amount of computational effort.

The specific differences between Kuprievich and Kudritskaya's (24) and our approach to the calculation of X_1^+ are the determination of an equilibrium geometry for the dimer and the manner in which ξ was changed. The equilibrium geometry of Kuprievich and Kudritskaya (24) was found as follows. The relative arrangement of nuclei in each of the dimer molecules was assumed to be the same as observed in a free formamide molecule (see Table I). The mutual orientation of the two molecules was constrained so that the atoms $C_1{=}O_1{---}H_4{-}N_2$ lay on a straight line (see Figure 18b). The equilibrium intermolecular distance was taken as that corresponding to the minimum total energy along the $C_1{=}O_1{---}H_4{-}N_2$ axis.

Our equilibrium geometry was derived from an energy minimization of the complete geometry of the dimer. This calculation took approximately 10 hours of CPU time and was accomplished utilizing energy gradient and optimization routines. The only constraint on the geometry optimization was that the dimer had to be planar. This constraint was implemented because the observed geometry of the formamide monomer is planar (see Table I and Ref. (40)).

The change in ξ should correspond to the motion of the carbon and oxygen atoms in the $C_1{=}O_1$ bond stretching motion. Kuprievich and Kudritskaya (24) chose to move only the O_1 atom in increments of -0.02 Bohr, so that E was calculated at the points ξ=0.0, -0.02, and -0.04 Bohr. The reason for the choice of two negative values of ξ is that the observed C=O bond length of 1.243Å (41) used as their equilibrium value is longer than the one calculated using the STO-3G basis set (1.219Å) (see Table I).

We elected to move both the O_1 and C_1 atoms in increments of 0.01 Bohr, so that E was calculated at ξ=0.0, 0.02, and 0.04 Bohr. Note that the molecular fragment attached to the C_1 atom (atoms N_1, H_1, H_2, and H_3 in Figure 18b) was also moved rigidly with the C_1 atom. Our motivation for moving both the O_1 and C_1 atoms was that this motion is in better agreement with the amide-I vibrational normal mode for the formamide monomer shown in Figure 18c.

C. RESULTS

Calculated and observed equilibrium internal coordinates and ground state dipole moments for the formamide dimer and monomer are given in Table I. The calculated ground electronic state properties used to determine X_1^+ for the formamide dimer are presented in Table II. Table III lists Kuprievich and Kudritskaya's (24) and our calculated values of X_1^+ for different harmonic force constants for the C=O bond stretch vibration in the formamide dimer and monomer.

Equilibrium Geometry

No experimental data are available on the geometry of the formamide dimer shown in Figure 18b. In order to estimate the accuracy of our energy-minimized geometry of the formamide dimer calculated using the STO-3G basis set, we calculated an energy-minimized geometry for the formamide monomer, on which there is experimental data (40). As in the case of the dimer, the monomer was constrained to be planar (designated STO-3G planar in Table I). We see in Table I that, except for the longer C_1-N_1 bond length, our calculated geometry does not differ significantly from the observed geometry given in the rightmost column of Table I, or from the geometry calculated using the ab initio SCF MO procedure with the more elaborate 4-31G split valence basis set (42). We conclude that our calculated equilibrium geometry for the formamide dimer is reasonable with the exception of the C_1-N_1 and C_2-N_2 bond lengths. Most importantly, the calculated C_1=O_1 bond length of 1.218 Å in the formamide monomer is in very good agreement with observed one at 1.219 ± 0.012 Å (40).

The equilibrium geometry of the formamide dimer constructed by Kuprievich and Kudritskaya (24) is given in the column headed by STO-3G + Obs. The internal coordinates for the formamide molecules in the dimer were taken from the experimental investigation of the formamide monomer by Kurland and Wilson in 1957 (41). Although there is a slight difference in the C_1=O_1 bond length, Kurland and Wilson's (41) results agree with the more recent spectroscopic study by Hirota, et. al in 1974 (rightmost column in Table I) (40). The hydrogen bond length ($r_{O_1}...H_4$) calculated by Kuprievich and Kudritskaya (1.853 Å) (24) and the present work (1.851 Å) are essentially identical. However, we calculate the O_1---H_4-N_2 bond angle to be slightly bent at 175° while Kuprievich and Kudritskaya (24) constrained it to be 180°. This difference should not be too significant, because the potential energy curve associated with the bending of hydrogen bonds is very shallow (24).

The Nonresonance Exciton-Phonon Interaction Parameter, X_1^+

The calculation of X_1^+ by Kuprievich and Kudritskaya (24) and the present work can be followed by reading Table II from left to right. Note that R in Table II is equivalent to $R_{m,\ m+1}$ in the text. We see that the values of K calculated by

Kuprievich and Kudritskaya (34) (1518 Nt/m at ΔR=0.0 Bohr and 1428 Nt/m at ΔR=0.66653 Bohr) are less than that of the present work (1585 Nt/m at ΔR=0.0 Bohr and 1578 Nt/m at ΔR=0.66653 Bohr). Furthermore, the change in K with respect to the change in R is calculated to be much greater by Kuprievich and Kudritskaya (-90 Nt/m) (24) than the present work (-7 Nt/m). In other words, Kuprievich and Kudritskaya (24) have calculated a greater perturbative effect of the motion of the H_4 atom (the acoustical phonon) upon the C_1=O_1 bond stretching vibration (the amide-I exciton) than is determined by our computations. This result is summarized in Table III which reveals the approximately one order of magnitude difference between the nonresonance exciton-phonon coupling parameter calculated by Kuprievich and Kudritskaya (24) (-2.65 to -3.64 x 10^{-11}Nt) and the present work (-0.20 to -0.27 x 10^{-11}Nt).

D. CONCLUSIONS

According to Scott (18) Davydov soliton formation in an alpha-helix is possible only when the magnitude of the nonresonance exciton-phonon interaction parameter exceeds a threshold equal to 3.5 x 10^{-11}Nt. The numerical analysis of Kuprievich and Kudritskaya (24) shows that the magnitude of X_1^+ can exceed such a threshold (see Table III). This result would provide support of the existence of solitons in polypeptide chains. However, our calculated magnitude of X_1^+ is an order of magnitude less than that derived by Scott (18), and it would argue against the existence of solitons in polypeptide chains.

The disagreement between Kuprievich and Kudritskaya's (24) calculated value for X_1^+ and ours was disturbing, and so we recalculated X_1^+ using the exact procedure of Ref. (24). We found that Kuprievich and Kudritskaya were in error. Instead of 3 x 10^{-11}Nt, their calculated magnitude of X_1^+ should be 0.7 x 10^{-11}Nt. Although 0.7 x 10^{-11}Nt is larger than our original calculated magnitude of 0.2 x 10^{-11}Nt, it still is less than the minimum value of 3.5 x 10^{-11}Nt predicted by Scott (18) to sustain a Davydov soliton. Thus, neither the STO-3G calculation in Ref. (24) nor ours supports the existence of Davydov solitons in hydrogen-bonded polypeptide chains.

A more sophisticated ab-initio - SCF-MO calculation employing the 4-31G basis set (42) yielded a magnitude of 1.3 x 10^{-11}Nt for X_1^+ (see Appendix I). This magnitude is less than Scott's minimum value (18), but it has increased relative to the one calculated using the STO-3G basis set. Therefore, as one improves the sophistication of the ab-initio -SCF-MO calculation, one would expect X_1^+ to to increase. It is necessary to improve the sophistication of the ab-initio - SCF-MO procedure, because of the complexity of the hydrogen bond involved in the exciton-phonon interaction (see Appendix I). As a result, the question concerning the presence of Davydov solitons in alpha-helical polypeptides still can not be answered definitively on the basis of the quantum mechanical calculations performed to date.

Table I.

TABLE I. Calculated and observed equilibrium internal coordinates and ground state dipole moments for the formamide dimer[a] and monomer[a]

Parameter[b]	Formamide dimer		Formamide monomer			
	STO-3G planar[c]	STO-3G+Obs.[d]	STO-3G planar[e]	STO-3G[f]	4-31G[g]	Obs.[h]
$r_{C_1 O_1}$ (Å)	1.219	1.243	1.218	1.215	1.216	1.219 ± 0.012
$r_{C_1 N_1}$ (Å)	1.397	1.343	1.403	1.437	1.347	1.352 ± 0.012
$r_{N_1 H_1}$ (Å)	1.014	0.995	1.014	1.026	0.990	1.002 ± 0.003
$r_{N_1 H_2}$ (Å)	1.015	0.995	1.015	1.027	0.993	1.002+0.003
$r_{C_1 H_3}$ (Å)	1.105	1.094	1.105	1.104	1.081	1.098 ± 0.010
$\angle N_1C_1O_1$ (deg)	124.4	123.6	124.4	124.0	124.9	124.7 ± 0.3
$\angle N_1C_1H_3$ (deg)	111.7	103.9	111.4	111.9	113.8	112.7 ± 2.0
$\angle H_3C_1O_1$ (deg)	123.9	132.5	124.3	124.0	121.3	122.6 ± 2.0
$\angle C_1N_1H_1$ (deg)	121.2	120.5	121.2	112.1	121.8	120.0 ± 0.5
$\angle C_1N_1H_2$ (deg)	120.6	120.5	120.5	111.7	119.6	118.5 ± 0.5
$\angle H_1N_1H_2$ (deg)	118.2	119.0	118.3	110.1	118.6	121.5 ± 0.5
$r_{O_1H_4}$ (Å)	1.851	1.853				
$r_{O_1N_2}$ (Å)	2.866	2.848				
$\angle O_1H_4N_2$ (deg)	175.0	180.0				
$r_{C_2 O_2}$ (Å)	1.220	1.243				
$r_{C_2 N_2}$ (Å)	1.396	1.343				
$r_{N_2 H_4}$ (Å)	1.017	0.995				

TABLE I. (Cont)

Parameter[b]	Formamide dimer STO-3G planar[c]	Formamide dimer STO-3G+Obs.[d]	Formamide monomer STO-3G planar[e]	Formamide monomer STO-3G[f]	Formamide monomer 4-31G[g]	Formamide monomer Obs.[h]
$r_{N_2 H_5}$ (Å)	1.014	0.995				
$r_{C_2 H_6}$ (Å)	1.106	1.094				
$\angle N_2C_2O_2$ (deg)	125.0	123.6				
$\angle N_2C_2H_6$ (deg)	111.2	103.9				
$\angle H_6C_2O_2$ (deg)	123.9	132.5				
$\angle C_2N_2H_4$ (deg)	121.4	120.5				
$\angle C_2N_2H_5$ (deg)	119.6	120.5				
$\angle H_4N_2H_5$ (deg)	119.0	119.0				
$\lvert\underline{\mu}\rvert$ (D)	6.28	na	2.64	na	4.47	3.71 ± 0.06
$\theta(\underline{\mu}, \Sigma c_i - u_i)$ (deg)	39.0	na	39.3	na	41.5	39.6

TABLE I. (cont)

a) The structure of the formamide dimer and the numbering of the atoms is given in Figure 18b. The formamide monomer is defined by the molecular fragment composed of atoms O_1, C_1, N_1, H_1, H_2, and H_3 in Figure 18b.

b) $r_{xy} \equiv$ bond length between atoms x and y; $\angle_{xyz} \equiv$ angle between the x-y and y-z bonds; $|\underline{\mu}| \equiv$ magnitude of the ground state dipole moment; $\Theta(\underline{\mu}, \underline{r}_{C_1-N_1}) \equiv$ angle between the C_1-N_1 bond vector and the ground state dipole moment vector. Note that na $\equiv$ not available.

c) This work. The geometry of the formamide dimer was determined by minimizing the energy of the molecular system with respect to the atomic coordinates. The energy was calculated using the ab initio self-consistent field (SCF) molecular orbital (MO) method with the STO-3G minimal atomic orbital basis set. Planar means that all the atoms in the dimer were constrained to remain in one plane during the optimization calculation.

d) Ref. 24. The geometry of the formamide dimer was determined in two parts: (1) the internal coordinates of the two formamide monomer units were taken to be identical and are the observed values for the formamide monomer given in Ref. 41; (2) the energy of the dimer was minimized with respect to the $r(O_1 \ldots H_4)$ distance, where the C_1, O_1, H_4, and N_2 atoms were constrained to be on one line. This energy was calculated using the ab initio SCF MO method with the STO-3G basis set.

e) This work. See c) with the exception that dimer is replaced by monomer.

f) Ref. 37. The geometry of the formamide monomer was determined by minimizing the energy of the molecule with respect to the atomic coordinates. The energy was calculated using the ab initio SCF MO method with the STO-3G basis set. The monomer was not constrained to remain planar in this calculation, and it was found that the minimum energy geometry was not planar with the O_1-C_1-N_1-H_1 and O_1-C_1-N_1-H_2 dihedral angles equal to 146.8° and 22.8°, respectively.

g) Ref. 37. The geometry of the formamide monomer was determined by minimizing the energy of the molecule with respect to the atomic coordinates. The energy was calculated using the ab initio SCF MO method with the 4-31G split-valence basis set. The monomer was calculated to be planar.

h) Ref. 40. A microwave spectrum of the formamide monomer in the gaseous state. The monomer was determined to be planar.

Table II

TABLE II. Calculated ground electronic state properties used to determine the non-resonance exciton-phonon coupling parameter in the formamide dimer[a)]

ΔR (Bohr)[b)]	ξ (Bohr)[c)]	E(Hartree)[d)] P e)	E(Hartree)[d)] KK f)	ΔE(Hartree x10^6)[g)] P e)	ΔE(Hartree x10^6)[g)] KK f)	Δ(ΔE)(Hartree x10^6)[h)] P e)	Δ(ΔE)(Hartree x10^6)[h)] KK f)	K (Nt/m)[i)] P e)	K (Nt/m)[i)] KK f)	ΔK/ΔR (Nt/m^2)[j)] P e)	ΔK/ΔR (Nt/m^2)[j)] KK f)
0.00000	0.00	-333.383404	-333.363548	280	-676						
	0.02	-333.383196	-333.364224	616	-286	408	390	1585	1518		
	0.04	-333.382580	-333.364510							-1.88	-25
0.66653	0.00	-333.381949	-333.361821	186	-605						
	0.02	-333.381763	-333.362426	592	-238	406	367	1578	1428		
	0.04	-333.381171	-333.362664								

TABLE II. (cont)

a) The structure of the formamide dimer is given in Figure 18b. The non-resonance exciton-phonon coupling parameter is defined in h) of Table III.

b) The change in hydrogen bond length ($r(O_1-H_4)$ in Figure 18b) with respect to its equilibrium value. A positive ΔR reflects an increase in $r(O_1-H_4)$.

c) The magnitude of the change in the carbonyl bond length ($r(C_1=O_1)$ in Figure 18b) with respect to its equilibrium value. Note that a positive/negative ξ reflects an increase/decrease of $r(C_1=O_1)$.

d) The total ground electronic state energy of the dimer.

e) The present work is represented by P. The ab initio self-consistent field (SCF) molecular orbital (MO) method with the STO-3G minimal atomic-orbital basis set was used to calculate the total energy of the dimer as a function of ΔR and ξ. Note the following: (1) ξ was positive, as it was increased in increments of 0.02; (2) ξ was increased by moving the O_1 atom and the molecular fragment composed of the C_1, N_1, H_1, H_2, and H_3 atoms (see text).

f) The work of Kuprievich and Kudritskaya in Ref. 24 is represented by KK. The ab initio SCF MO method with the STO-3G basis set was used to calculate the total energy of the dimer as a function of ΔR and ξ. Note the following: (1) ξ was negative, as it was decreased in increments of 0.02; (2) ξ was decreased by moving only the O_1 atom (see text); (3) the total energy of the dimer decreases as ξ decreases, because the initial $r(C_1=O_1)$ = 1.243 Å is greater than the optimal $r(C_1=O_1)$ = 1.219 Å calculated using the ab-initio SCF MO method with the STO-3G basis set (see text and Table I).

g) The change in total energy associated with the change in ξ ($\Delta\xi$).

h) The change in ΔE associated with $\Delta\xi$.

i) The estimate of the diagonal force constant for the stretching of the $C_1=O_1$ bond. $K = \partial^2 E/\partial\xi^2 \cong \Delta(\Delta E)/(\Delta\xi)^2$.

j) The third derivative of the total energy of the dimer which is the crucial component of the non-resonance exciton-phonon coupling parameter (see text and Table III).

TABLE III. Calculated values of the non-resonance exciton-phonon coupling parameter for different diagonal force constants for the C = O bond in the formamide dimer[a] and monomer[a]

K(Nt/m) [b]	X_1^+(Nt x 10^{11}) [h]	
	P [i]	KK [j]
1150	-0.27	-3.64
(monomer, Ref. 40)[c]		
1380	-0.22	-3.03
(monomer, Ref. 37)[d]		
1540	-0.20	-2.72
(monomer, Ref. 24)[e]		
1473	-0.21	-2.84
(dimer, Ref. 24)[f]		
1581	-0.20	-2.65
(dimer, This work)[g]		

TABLE III. (cont)

a) The structure of the formamide dimer is given in Figure 18b. The formamide monomer is defined by the molecular fragment composed of atoms O_1, C_1, N_1, H_1, H_2, and H_3 in Figure 18b.

b) The diagonal force constant for the stretching of the $C_1=O_1$ bond.

c) Derived from spectroscopic data.

d) Calculated using the ab-initio self-consistent field (SCF) molecular orbital (MO) method with the 4-31G split-valence basis set.

e)-g) Calculated using the ab-initio SCF MO method with the STO-3G basis set.

h) The non-resonance exciton-phonon coupling parameter.

$X_1^+ \cong \frac{\hbar\omega}{2K} \frac{\partial K}{\partial R} \cong \frac{\hbar\omega}{2K} \frac{\Delta K}{\Delta R}$, where $\hbar\omega$ = the experimental mean frequency of the amide-I vibration (1660 cm^{-1} = 3.297 x 10^{-20}J), K as defined in b), and $\Delta K/\Delta R$ as defined in i) of Table II.

i) The value of X_1^+ determined using $\Delta K/\Delta R$ calculated in the present work.

j) The value of X_1^+ determined using $\Delta K/\Delta R$ calculated by Kuprievich and Kudritskaya in Ref. 24.

References

(1) Kremer, F. and A. Keilman, (1983), Phys. Rev. Lett. 50:1766.

(2) Furia, L., O. Gandhi, and D. Hill (1983), in Coherent Excitations in Biological Systems, Springer - Verlag, New York.

(3) Kremer, F., C. Koschnitzke, L. Santo, P. Quick and A. Poglitsch (1983), in Coherent Excitations in Biological Systems, Springer - Verlag, New York.

(4) Wasieliwski, M., C.H. Bok, M. Bowman and J. Norris (1983), Nature 303:520.

(5) Adey, W.R. (1981), Physiol. 61:435.

(6) Adey, W.R.(1984), in Proceedings of the Loma Linda Conference on Nonlinear Electrodynamics in Biological Systems, Plenum Press, New York.

(7)
a. Johnston, C. (1984), Private Communication.

b. Johnston, C. (1984), Chem Phys. Letters (To Appear).

(8) Davydov, A.S., (1977), Studia Biophysica. 62:1.

(9) Peticolas, W.L. (1979), in Methods of Enzymology (Academic Press), 61:425-458.

(10) Northrup, S.H., M.R. Pear, C.-Y. Lee, J.A. McCammon, and M. Karplus, (1982), Proc. Natl. Acad. Sci USA, 79:4035-4039.

(11) Sheridan, R.P. R.M. Levy, and S.W. Englander, (1983), Proc. Natl. Acad. Sci. USA, 80:5569-5572

(12) McCammon, J.A. and M. Karplus, (1983), Acc. Chem. Res., 16:187-193.

(13) Pain, R.H., (1983), Nature, 305:581-582.

(14) Go. N., T. Noguti, T. Nishikawa, (1983), Proc. Natl. Acad. Sci. USA, 80:3696-3700.

(15) Brooks, B. and M. Karplus, (1983), Proc. Natl. Acad. Sci. USA, 80:6571-6575.

(16)
a. Davydov, A.S., (1979), Physica Scripta, 20:387-394.

b. Davydov, A.S., (1979), Acad. Sci Ukranian SSR, Inst. for Theor. Physic, Preprint ITP-79-69E.

(17) Hyman, J.M. D.W. McLaughlin, and A.C. Scott, (1981), Physica 3D:23-44.

(18) Scott, A.C. (1982), Phys. Rev. A, 26:578.

(19) Lomdahl, P.S., (1983), in Proceedings of the Loma Linda Conference on Nonlinear Electrodynamics in Biological Systems Plenum Press. (To Appear).

(20) Green, D.E., (1973), Science 181:583.

(21) Green, D.E., (1974), Ann. N.U. Acad. Sci. 227:6.

(22) Davydov, A.S., A.A. Eremko, and A.I. Sergienko, (1978), Ukran. Fix. Zh. 23:983.

(23) Ovchinnikov, A.A. and N.S. Erikhman, (1982), Sov. Phys. Usp. 25:738.

(24) Kuprievich, V.A. and Z.G. Kudritskaya, (1982), Preprint ITP-82-64E, Institute for Theoretical Physics, Kiev.

(25) Careri, G., U. Bontempo, F. Carta, E. Gratton, and A.C. Scott, (1983), Phys. Rev. Lett. 51:304.

(26) Munn, R.W. and R. Silbey, (1978), J. Chem. Phys. 68:2439.

(27) Davydov, A.S., (1980), Zh. Eksp. Teor. Fiz. 78:789.

(28) Davydov, A.S. (1983), Sov. Phys: Usp. 25:898.

(29)
a. Fedyanin, V.K. and L.V. Yakushevich, (1977), Teor. Mat. Fiz. 30:133.

b. (1978), Teor. Mat. Fiz. 37:371.

(30) Shampiro, L.F. and S. Gordon (1975), Computer Solution of Ordinary Differential Equations , Academic Press, New York.

(31) Haaken, H. (1976), Quantum Field Theory of Solids , Chapter III. North-Holland, New York.

(32) Toda, M. (1981), Theory of Nonlinear Lattices , Springer - Verlag, New York.

(33) Flaschka, H. (1974), Phys. Rev. B29:1925.

(34) Kuprievich, V.A. and Z.G. Kudritskaya, (1982), Acad. Sci. Ukranian SSR, Inst. for Theor. Phys., Preprint ITP-82-63E.

(35) Schiff, L.I., (1968), Quantum Mechanics , McGraw-Hill New York.

(36) Evans, J.C. (1954), J. Chem. Phys., 22:1228-1234.

(37) Sugawara Y., Hamada, Y., Hirakawa, A.Y., Tsuboi, M., Kato, S., and Morokuma, K., (1980), Chem. Phys. Lett., 50:105-111.

(38) Schaefer, H.F., The Electronic Structure of Atoms and Molecules. A Survey of Rigorous Quantum Mechanical Results (1972), Addison-Wesley.

(39) Hehre, W.J., R.F. Stewart, and J.A. Pople, (1969), J. Chem. Phys., 51:2657-2664.

(40) Hirota, E., R. Sugisuki, C.J. Nielsen, and G.O. Sorensen, (1974), J. Molec. Spectors, 49:251-267.

(41) Kurland, R.J. and E.B. Wilson, (1957), J. Chem. Phys., 27:585-590.

(42) Ditchfield, R., W.J. Hehre, and J.A. Pople, (1971), J. Chem Phys., 54:724-728.

(43) Tanaku, Y. and K. Machida, (1976), J. Molec. Spect., 63:306-316

(44) Nevskaya, N.A. and Yu N. Chirgadze, (1976), Biopolymers, 15:637-648.

APPENDIX I. The calculation of the nonlinear coupling constant (X_1^+), using an ab-initio -SCF-MO procedure with the 4-31G basis set.

The calculation of X_1^+ using an ab-initio -SCF-MO formalism with the 4-31G split valence basis set is a great improvement over earlier calculations employing the STO-3G basis set (see Section III and Ref. I-1). However, before discussing the results of the 4-31G calculation, there is one finding to be noted concerning the STO-3G calculations; the magnitude of $X_1^+ = 3 \times 10^{-11}$Nt calculated by Kuprievich and Kudritskaya (I-1) is too high. We recalculated X_1^+ by following exactly the procedure outlined by Kuprievich and Kudritskaya (I-1), and obtained a magnitude equal to 0.7×10^{-11}Nt. Although Kuprievich and Kudritskaya (I-1) mention that they had SCF convergence problems (we had none), the errors in their calculation of X_1^+ are not clear to us. In conclusion, neither the STO-3G calculation in Ref. I-1 nor ours (Section III) yields a value of $|X_1^+|$ which exceeds the threshold of 3.5×10^{-11} Nt predicted by Scott (I-2). This result will be discussed in detail below.

Ab-initio -SCF-MO calculations of molecular properties employing the STO-3G basis set are crude. This fact is particularly true when treating interactions like X_1^+, which are associated with hydrogen bonding. The starting point for the treatment of hydrogen-bonded systems is to use the 4-31G basis set. It is stressed that this basis set is only the starting point because the van der Waals forces which are important in hydrogen bonding are not being described reasonably until one utilizes second and third order Møller-Plesset perturbation theory in conjunction with polarized basis sets of the 6-311G** type (I-3).

The ab-initio -SCF-MO calculation of X_1^+ using the 4-31G basis set followed the same procedure outlined for the calculation employing the STO-3G basis set: (1) use a formamide dimer as the simplest model of the polypeptide chain, (2) calculate an equilibrium geometry of the dimer, (3) calculate K or $K_{C=O}$ as a function of $R_{m,m+1}$ or $R_{O\ldots H}$. However, unlike the STO-3G calculation which determined $K_{C=O}$ at two values of $R_{O\ldots H} = 0.00$ and 0.35 Å, the 4-31G calculation computed $K_{C=O}$ at seven values of $R_{O\ldots H} = \pm 0.05, \pm 0.02, \pm 0.01$, and 0.00 Å.

Calculated (STO-3G and 4-31G) and observed equilibrium geometries of the formamide monomer are shown in the top part of Figure I-1. Note that the calculated geometries were constrained to be planar, and the observed one was found to be planar. It is clear that the 4-31G calculated geometry matches up better with the observed one than does the STO-3G calculated geometry. This observation is particularly true for the C_1-N_1 bond length. The term $|\underset{\sim}{\mu}|$ is the magnitude of the dipole moment, and $\theta(\underset{\sim}{\mu}, \underset{\sim}{r}_{C_1-N_1}) \equiv \theta$ is the angle between the dipole moment vector and C_1-N_1 bond vector.

Calculated (STO-3G and 4-31G) equilibrium geometries of the formamide dimer are shown in the bottom half of Figure I-1. No observed equilibrium geometry of the dimer is available in this configuration. Similar to that for the monomer, the calculated geometry of the dimer was constrained to be planar. The major points to be noted concerning the calculated dimer geometries are (1) the $R_{C_1=O_1}$ and $R_{H_4-N_2}$ in the dimer with respect to $R_{C_1=O_1}$ and $R_{H_1-N_1}$ in the monomer are greater for the 4-31G calculation (+ 0.005 and + 0.007 Å, respectively) than those for the STO-3G calculation (+ 0.001 and + 0.003 Å, respectively). Clearly, the formamide monomer is calculated in the 4-31G basis set to be more affected by hydrogen bonding than in the STO-3G basis set.

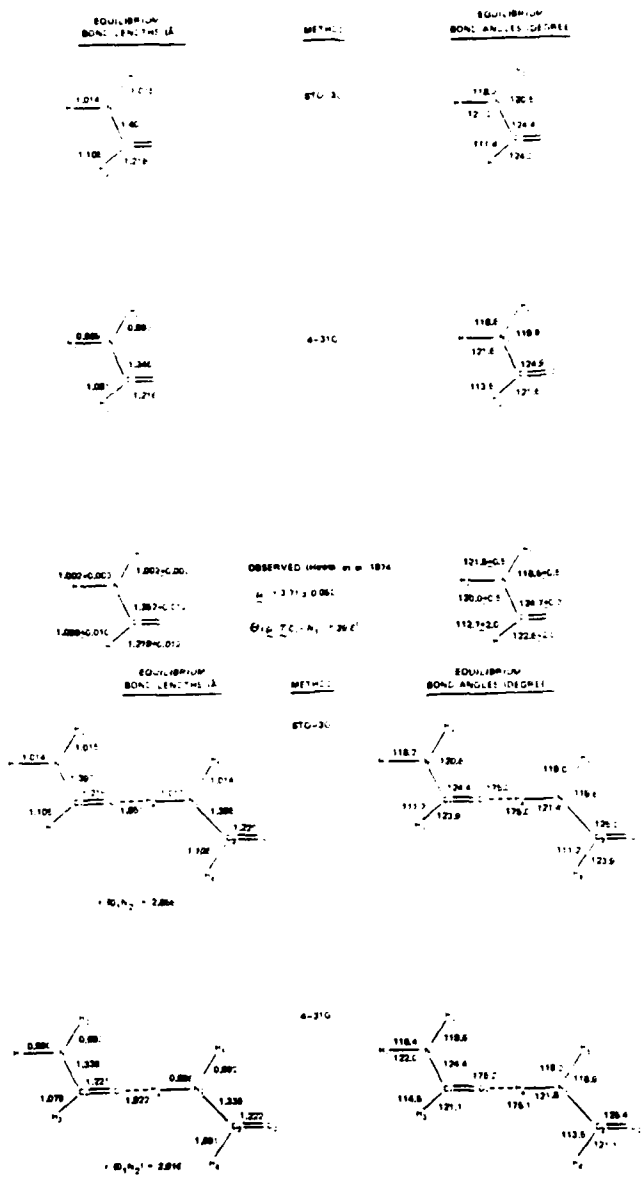

Figure I-1. Equilibrium geometries of the formamide monomer and dimer calculated using the ab-initio -SCF-MO procedure with the STO-3G and 4-31G basis sets. The observed geometry of the formamide monomer determined by Hirota, et . al (I-6) is also shown. Note that $|\underset{\sim}{\mu}|$ is the magnitude of the molecular diple moment, and $\theta\ (\underset{\sim}{\mu},\ \underset{\sim}{r}_{C_1-N_1})$ is the angle between the dipole moment vector and the C_1-N_1 bond vector.

Calculated (STO-3G and 4-31G) electronic charge distributions for the calculated equilibrium geometries of the formamide monomer are shown in the left-half of Figure I-2. The polarization of charges across all bonds increases as one goes from the STO-3G to the 4-31G basis set. It is also shown that the charge distribution for the formamide monomer calculated using the even more elaborate 6-31G basis set (I-4) is not too different from the 4-31G calculated charge distribution. This statement is supported further by noting that $|\underset{\sim}{\mu}|$ (4-31G) = 4.471D is closer in value to $|\underset{\sim}{\mu}|$ (observed) = 3.71 $\pm$ 0.06D than is $|\underset{\sim}{\mu}|$ (STO-3G) = 2.641D. Both θ (4-31G) = 41.3° and θ (STO-3G) = 39.3° are in near-agreement with θ (observed) = 39.6°.

Calculated (STO-3G and 4-31G) electronic charge distributions for the calculated equilibrium geometries of the formamide dimer are shown in the right-half of Figure I-2. As in the case of the formamide monomer, the polarization of charges across all bonds increases as one goes from the STO-3G to the 4-31G basis set. This observation is reflected in $|\underset{\sim}{\mu}|$ (4-31G) = 10.331D being greater than $|\underset{\sim}{\mu}|$ (STO-3G) = 6.280D. The greater polarization of charge across the hydrogen bond calculated using the 4-31G basis set implies a greater intermolecular interaction which should result in a greater value of $|X_1^+|$.

Figure I-3 presents the plot of $K_{C=O}$ vs. $R_{O\ldots H}$ calculated with the 4-31G basis set. The linear regression fit of the points yielded an equation, $K_{C=O} = 1463.1 - 97.5\ R_{O\ldots H}$, with an $r^2 = 0.993$. The slope of the plot yields a value of $X_1^+ = -0.13 \times 10^{-10}$Nt. The terms $_oX_1^+$, $K^{eq}_{C=O}$ (force constant for the calculated equilibrium geometry at $R_{O\ldots H} = 1.922$ Å), $\hbar\omega$ (amide-I frequency), E_{SCF} (total energy of the dimer), and Δ (binding energy of the dimer or hydrogen bond stabilization energy) calculated for the formamide dimer employing the 4-31G and STO-3G basis sets are given in Table I-I.

Although $|X_1^+|$ (4-31G) has increased relative to $|X_1^+|$ (STO-3G), it is still less than the minimum value of 0.35 10^{-10}Nt predicted by Scott (I-2) to sustain a Davydov soliton in alpha-helical polypeptides. However, since $|X_1^+|$ is proportional to the hydrogen bond binding energy (Δ in Table I-I), the stronger the hydrogen bond, the greater the value of $|X_1^+|$. There is no doubt that the hydrogen bond for the formamide dimer is stronger than what we have calculated using the 4-31G basis set, because we have neglected the van der Waals forces. Furthermore, the strength of hydrogen bonds between molecular units in a hydrogen-bonded polymer chain can be double that of the hydrogen bond in a dimer (I-5). Therefore, by including van der Waals forces in our theoretical formalism and by increasing the number of formamide monomer units in our model of the polypeptide, we would expect the calculated $|X_1^+|$ to increase to a value perhaps greater than 0.35×10^{-10}Nt. From the perspective of the quantum mechanical calculation of X_1^+, the question of the presence of Davydov solitons in alpha-helical polypeptides is still not resolved.

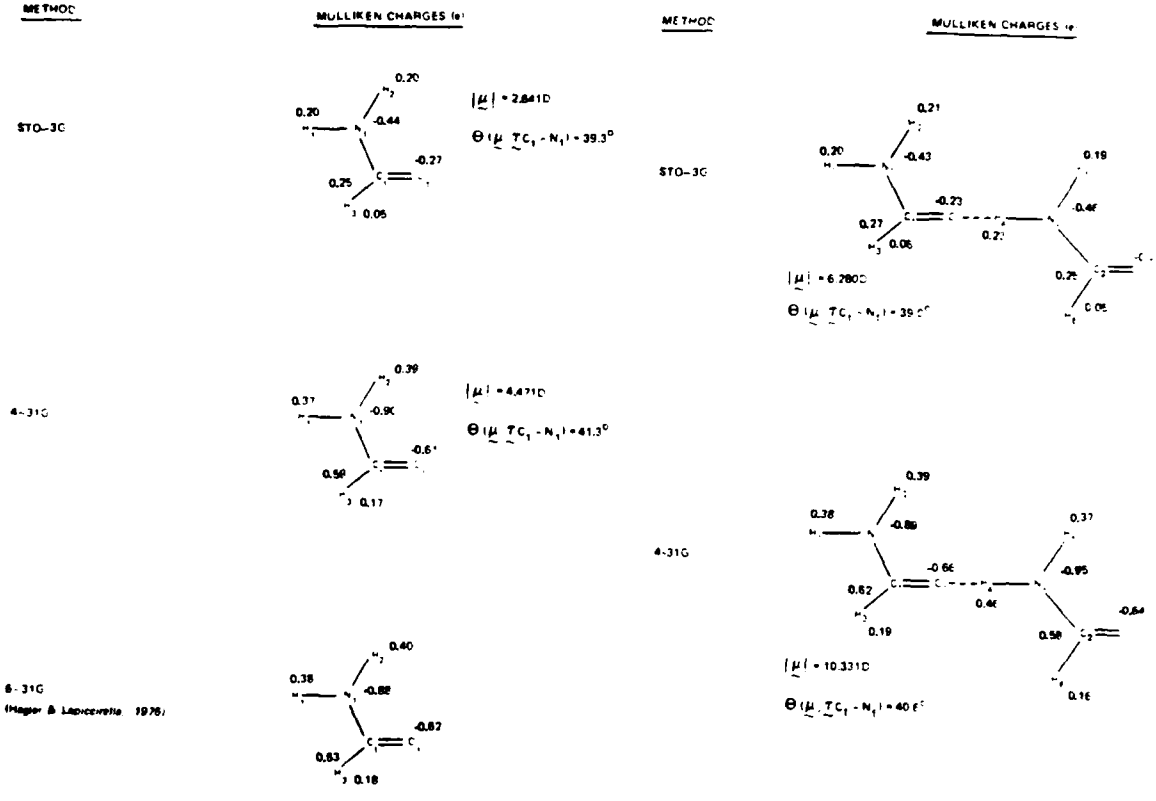

Figure I-2. Electronic charge distributions for equilibrium geometries of the formamide monomer and dimer calculated using the ab-initio -SCF-MO procedure with the STO-3G and 4-31G basis sets. The electronic charge distribution for the formamide dimer calculated by Hagler and Lapiccirella (I-4) with the 6-31G basis set is also shown. The terms $|\underset{\sim}{\mu}|$ and $\theta\,(\underset{\sim}{\mu}, \underset{\sim}{r}_{C_1-N_1})$ are defined in the caption to Figure I-1.

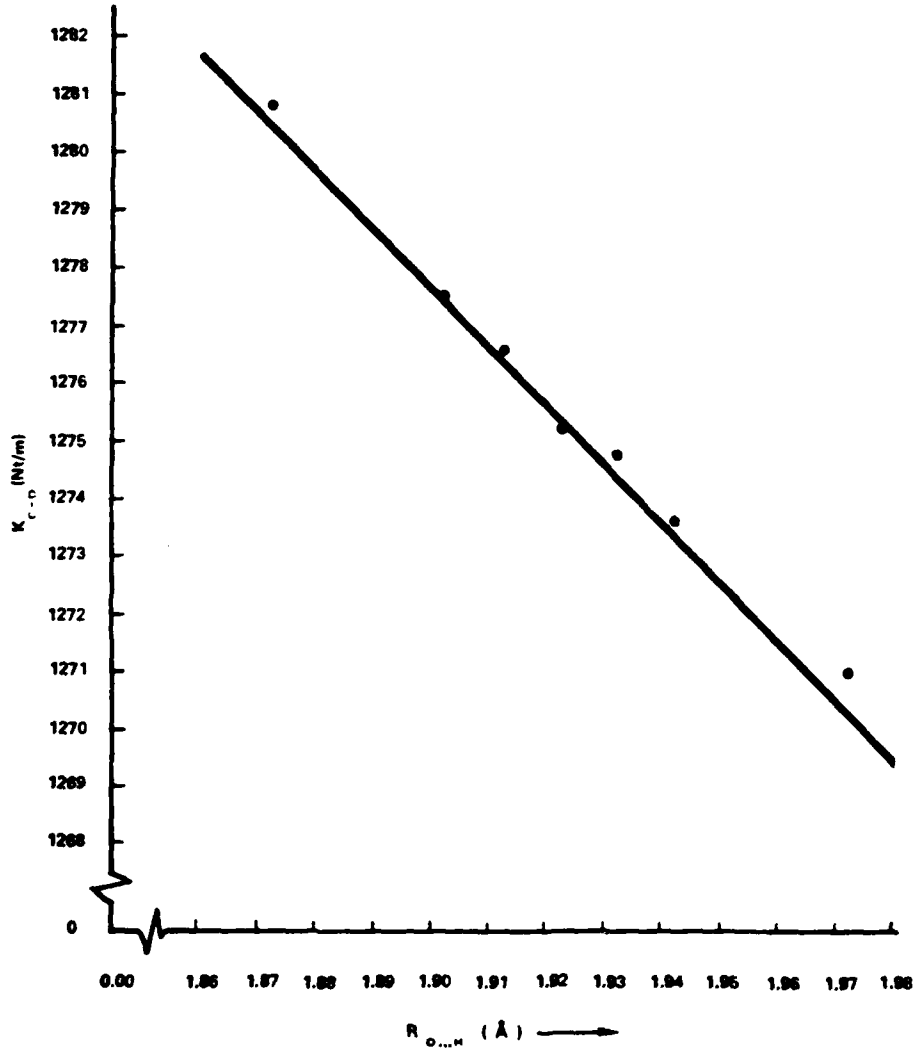

Figure I-3. A plot of the C=O stretching force constant ($K_{C=O}$) as a function of hydrogen bond length ($R_{O\cdots H}$) for the formamide dimer calculated using the ab-initio SCF-MO procedure with the 4-31G basis set. The equilibrium hydrogen bond length was calculated to be 1.922 Å (See Figure I-1).

TABLE I-I

Calculated values of the exciton-phonon coupling term (X_1^+) and related parameters for the formamide dimer.

PARAMETER	PRESENT WORK 4-31G	PRESENT WORK STO-3G	SCOTT, 1982[b]
X_1^+ (10^{10}Nt)	-0.13	-0.07	0.35
$K_{C=O}^{eq}$(Nt/m)	1275[c]	1553[c]	na
$\hbar\omega$(cm^{-1})	1660	1660	na
E_{SCF}(au)	-337.376457664	-333.383404267	na
Δ [a](eV)	-0.36168	-0.18984	na

(a) $\Delta = E_{SCF}$ (dimer) $-2E_{SCF}$ (monomer); na = not applicable

(b) A.C. Scott, Phys. Rev. A 26 , 578 (1982)

(c) $K_{C=O}^{eq}$ (4-31G, monomer) = 1285 Nt/m;

$K_{C=O}^{eq}$(STO-3G, monomer) = 1586 Nt/m.

REFERENCES FOR APPENDIX I

I-1. Kuprievich, V.A. and Z.G. Kudritskaya, (1982), Acad. Sci. Ukranian SSR, Inst. for Theor. Phys., Preprint ITP-82-64E.

I-2. Scott, A.C., (1982), Phys. Rev. A, 26:578-595.

I-3. Szczesniak, M.M and S. Scheiner, (1984), J. Chem. Phys., 30:1535-1542.

I-4. Hagler, A.T. and L. Lapiccirella, (1976), Biopolymers, 15:1167-1200.

I-5. Beyer, A., A. Karpfen, and P. Schuster, (1984), in Hydrogen Bonds , Topics in Current Chemistry, Vol. 120, Springer, New York.

I-6. Hirota, E., R. Sugisuki, C.J. Nielsen, and G.O. Sorensen, (1974), J. Molec. Spectros., 49:251-267.


DATE
ILME